Stability of Rectangular Connection Elements

BO DOWSWELL

ABSTRACT

Connection elements are commonly designed using the flexural buckling and lateral-torsional buckling provisions in AISC *Specification* Sections E3 and F11, respectively, as well as the combined-load requirements of Section H1. Because these provisions were developed for main members, their accuracy for designing connection elements is questionable. The factors affecting the stability of connection elements are discussed, with an emphasis on the differences between main members and connection elements. The available experimental and theoretical results are compared to the AISC *Specification* equations. Where required, new equations are derived, and practical design solutions are recommended. Recommendations are also made for connection elements subjected to combined axial and flexural loads. Examples are provided to illustrate the proposed design procedures for double-coped beams.

Keywords: connections, rectangular elements, stability, flexural buckling, lateral-torsional buckling.

INTRODUCTION

In design, simplifying assumptions are required to reduce complex problems to idealized models with well-documented solutions and predictable behavior. Connections are often divided into rectangular elements, which are modeled as beams, columns and tension members. However, connection elements may not behave the same as the main members in a structure due to smaller length-to-depth ratios, unpredictable stress distributions, ambiguous boundary conditions, different residual stress patterns, and large out-of-flatness tolerances. These differences are usually insignificant for compact connection elements, where yielding is the primary limit state; however, they may be detrimental to connection elements subject to buckling.

AISC *Specification* (AISC, 2010a) Sections E3 for flexural buckling, F11 for lateral-torsional buckling, and H1 for combined loads were developed for designing main structural members. Although the applicability of these *Specification* provisions for the design of connection elements has not been verified, they are commonly used to design gusset plates and other connection elements. Inaccuracies in connection design models caused by adapting member design equations to connection elements can lead to a reduction in stability.

The purpose of this paper is to determine the accuracy of the AISC *Specification* stability provisions for designing rectangular connection elements. The factors affecting the stability of connection elements are discussed, with an emphasis on the differences between main members and connection elements. The available research relevant to the stability of connection elements is reviewed, and the available experimental and theoretical results are compared to the AISC *Specification* equations. Where required, new equations are derived and practical design solutions are recommended.

Bo Dowswell, P.E., Ph.D., Principal, ARC International, LLC, Birmingham, AL. Email: bo@arcstructural.com

Paper No. 2014-19

CONNECTION DESIGN MODELS

Several existing solutions are available, where the effective length factors, K, and lateral-torsional buckling modification factors, C_b, have been calibrated with experimental and/or finite element results. Some of these solutions are presented in a qualitative manner to provide background information on the applicability of *Specification* Sections E3, F11 and H1 to the design of connection elements.

Gusset Plates in Compression

Thornton (1984) proposed a method to calculate the flexural buckling strength of corner gusset plates (Figure 1a), where the gusset plate is modeled as a rectangular column as shown in Figure 1b. The buckling strength is calculated using the equations in Section E3 of the AISC *Specification*. As experimental and finite element data became available, the effective length factors were calibrated to provide more accurate solutions (Dowswell, 2006; Dowswell, 2012a).

Lapped Gusset Plates in Compression and Flexure

Due to a high level of erection efficiency, HSS bracing connections are sometimes fabricated using lapped gusset plate connections, shown in Figure 2a. The connection consists of a lug plate shop welded to a slot on the HSS brace centerline, which is field bolted to the gusset plate. The eccentricity

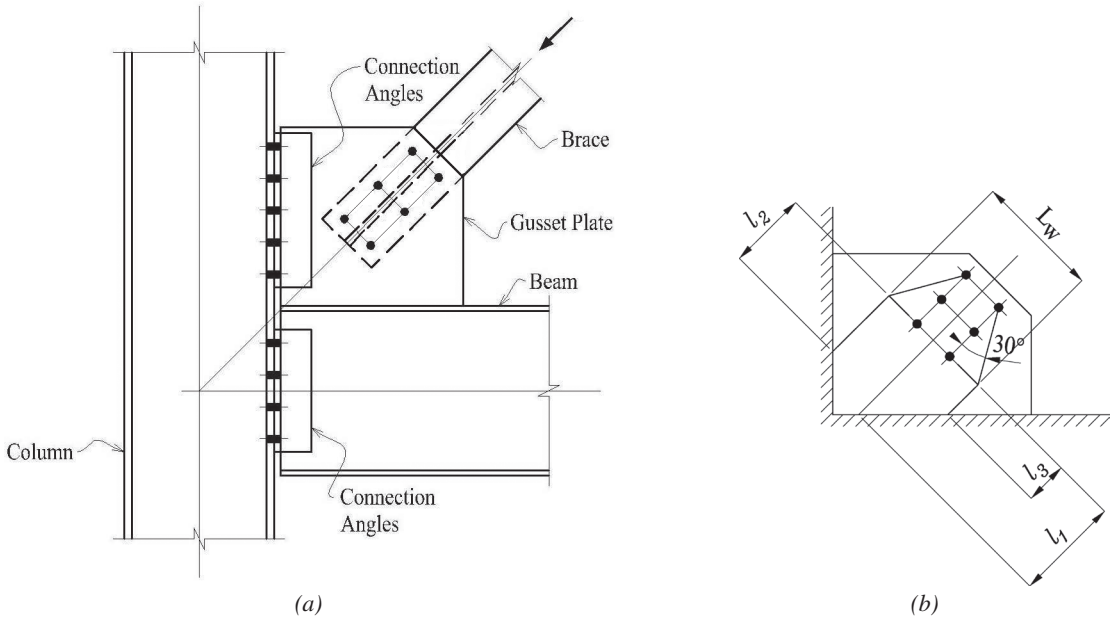

Fig. 1. Gusset plate in compression: (a) cover gusset plate; (b) equivalent column.

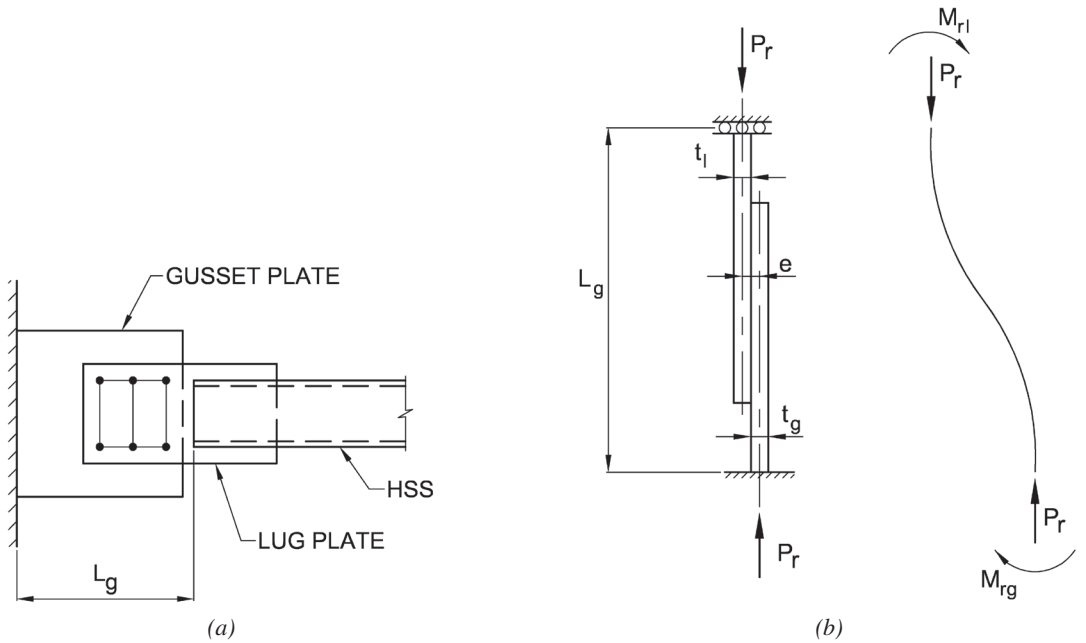

Fig. 2. Lapped gusset plate in compression and flexure: (a) lapped gusset plate; (b) equivalent beam-column.

between the centerline of the brace and the center of the gusset plate causes an eccentricity that significantly lowers the compression strength of the connection.

In AISC Design Guide 24 Hollow Structural Section Connections (Packer et al., 2010), the plates are modeled as a beam-column as shown in Figure 2b. The buckling strength is calculated using the beam-column provisions of AISC *Specification* Section H1 and the flexural buckling provisions in Section E3. This beam-column model was first published in the AISC *Hollow Structural Sections Connections Manual* (AISC, 1997). Clifton (2006), Clifton et al. (2007), Albermani et al. (2009), Hogan and Collins (2010), and Wilkinson et al. (2010) have refined the design procedure.

Double-Coped Beams

In beam-to-girder connections, the beam is usually coped to allow a standard connection to the girder web. If the beam and girder are of equal depth, both flanges must be coped as shown in Figure 3a. Due to the flexural and shear stresses in the coped portion of the web, web buckling can limit the local strength.

The AISC *Steel Construction Manual* (AISC, 2011) provides a semi-empirical design procedure for localized stability of double-coped beams. The AISC *Manual* procedure was developed by Cheng et al. (1984) by modeling the cope as a cantilever beam with a length equal to the cope length, *e*, as shown in Figure 3b. Dowswell and Whyte (2014) developed equations for lateral-torsional buckling modification factors, C_b, for use with the lateral-torsional buckling provisions in Section F11 of the AISC *Specification*.

Wrap-Around Gusset Plates

Where a horizontal brace is located at a beam-to-column intersection, the gusset plate must be cut out around the column as shown in Figure 4a. Due to the unconventional geometry, flexural stresses develop in the plate that must be accounted for in design. The assumed load distribution in wrap-around gusset plate connections is shown in Figure 4b, where the moment varies linearly along the length of each leg, and the maximum moment is at the reentrant corner.

Dowswell (2005) showed that the strength of each leg can be calculated based on an equivalent cantilever beam model. Dowswell (2012b) recommended using the lateral-torsional buckling provisions in Section F11 of the AISC *Specification* with different buckling lengths that were based on experimental behavior.

FACTORS AFFECTING STABILITY OF CONNECTION ELEMENTS

The primary factors influencing the stability of connection elements, such as buckling length and sectional properties, are explicitly addressed in the equations of *Specification* Sections E3 and F11. Other factors, including material and geometric imperfections, were considered in the development of the equations; however, the influence of these variables is defined only implicitly.

Although some imperfections can be beneficial, they usually have a detrimental effect on connection stability. Buckling strength decreases with increasing geometric imperfections, which are typically much larger for connection elements than for main members. Compression residual stresses decrease the elastic range of behavior, causing a decrease in buckling strength.

Geometric Imperfections

Although the AISC *Code of Standard Practice* (AISC, 2010b) requires a maximum out-of straightness of $L/1{,}000$ for straight compression members, the column curve in AISC *Specification* Section E3 was developed for column shapes with an initial out-of-straightness of $L/1{,}500$ (Bjorhovde, 1988). This is because Bjorhovde (1988) calculated an average out-of-straightness of $L/1{,}500$ for wide flange shapes used in North America, where L is the length between points of lateral support. For lateral-torsional buckling, AISC *Specification* Section F11 was developed based on a geometrically perfect member.

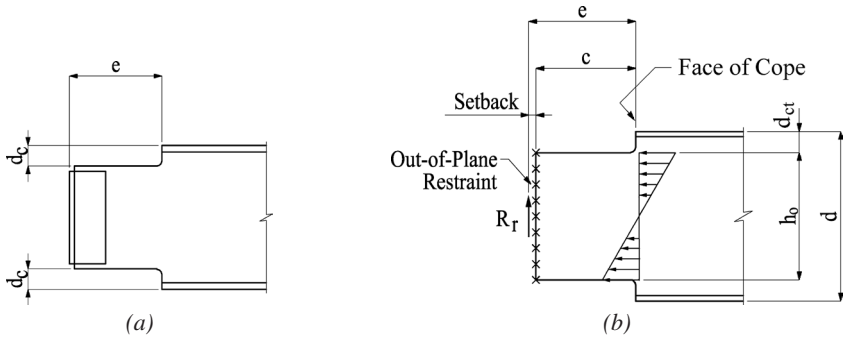

Fig. 3. Double-coped beam: (a) double-coped beam; (b) design model.

Geometric imperfections in connection elements can come from mill tolerances, fabrication operations, shipping damage, or distortion caused by pulling out-of-tolerance members together during erection. The out-of-flatness of connection elements are usually much larger than the out-of-straightness of a typical column when expressed as the imperfection-to-buckling length ratio. However, there are no standard tolerances for in-place connection elements. ASTM A6 (ASTM, 2013) specifies a permissible camber of 0.025 in./ft and a permissible variation from flat of 0.25 in. for carbon steel plates less than 36 in. long. This is equivalent to a permissible out-of-flatness of $L/480$, which is twice the permissible out-of-straightness of columns less than 30 ft long. The ASTM standard is applicable only to manufacturing tolerances and does not address the tolerances for plates after fabrication and erection is complete. Fouad et al. (2003) surveyed state departments of transportation, manufacturers and engineers to determine the current state of practice regarding flatness tolerances for connection plates and base plates. They recommended using the flatness requirements of ASTM A6 as a post-fabrication tolerance. Because geometric imperfections can significantly reduce the buckling strength of connection elements, they must be considered in the development of design recommendations.

Residual Stresses

Residual stresses are self-equilibrating stresses that are built into members as a result of the manufacturing and fabrication operations. Thermal residual stresses are caused by uneven cooling of the material after hot rolling, welding, and flame cutting. For bars and universal mill (UM) plates with rolled edges, the across-width residual stress pattern is shown in Figure 5a.

Welded and flame-cut members have tensile residual stresses at the location of the heat input. Plates with thermally cut edges have a residual stress pattern that varies across the width as shown in Figure 6a, with very high tensile residual stresses at the cut edges and balancing compression residual stresses at the center of the width.

According to Bjorhovde et al. (2001), the magnitude of the tension residual stress for oxyfuel thermal cutting is "generally around 60 to 70 ksi, regardless of the original material properties." This was confirmed by Spragen and Claussen (1937), Rao and Tall (1961), Tall (1964), Dwight and Ractliffe (1967), McFalls and Tall (1969), and Bjorhovde et al. (1972). Dwight and Ractliffe (1967), Young and Dwight (1971), and Dwight and Moxham (1977) used a simplified residual stress pattern in their studies, where the curved pattern was replaced with the rectangular stress blocks shown in Figure 6b. Due to the lower heat input typical of plasma cutting, tensile residual stress for plasma-cut edges are typically less than half of the material yield strength (Harris, 1997).

Most connection material is thermally cut, with grinding if required to remove imperfections. Residual stresses due to grinding are dependent on several factors, such as wheel speed, abrasive roughness, grinding direction, and use of coolant. In typical structural fabrication shops, handheld angle grinders are used with no coolant, which creates tensile residual stresses due to uneven cooling (Harvey, 1985). Measurements by Blehaut et al. (2002) showed tension residual stresses at the ground surface between 20 and

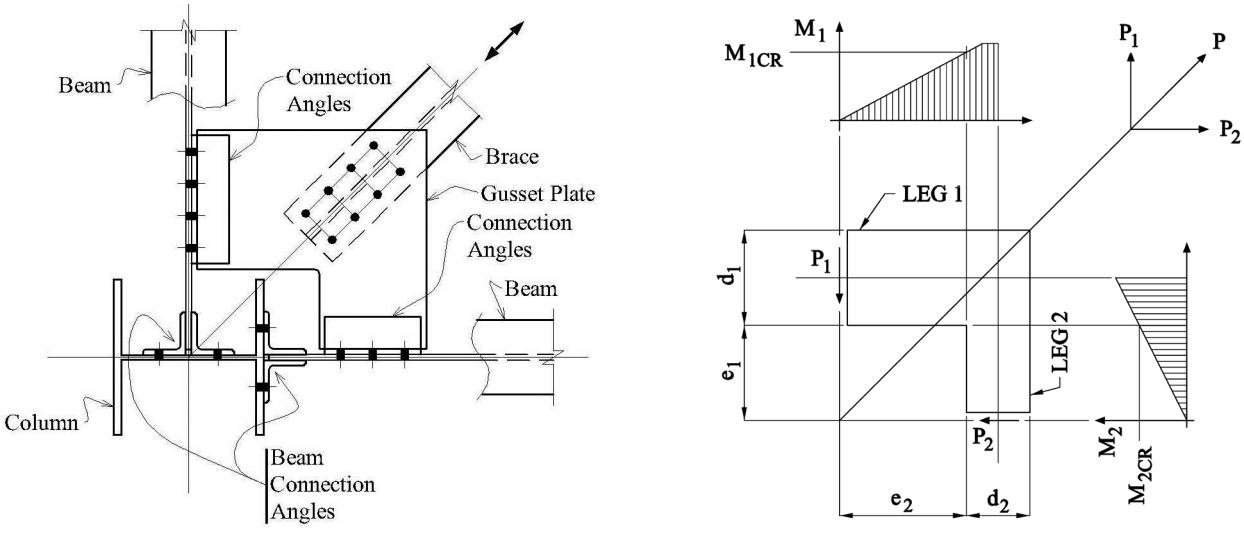

Fig. 4. Wrap-around gusset plate: (a) wrap-around gusset plate; (b) load system.

64 ksi, with the lower values perpendicular to the grinding direction.

Through-thickness residual stress patterns can be determined from the two-dimensional mapping of measured residual stresses by Alpsten (1968) and Alpsten and Tall (1969). For bars and UM plates, the pattern in Figure 7a provides a reasonable fit to the data from Alpsten (1968). For flame-cut plates, the pattern in Figure 7b is based on the data from Alpsten and Tall (1969).

Because residual stresses must be in equilibrium across any plane, the through-thickness and across-width residual stresses are interdependent. Due to this, the through-thickness residual stress distribution varies along the plate width. Both the Alpsten (1968) specimens and the Alpsten and Tall (1969) specimens had small aspect ratios (between 7 and 8); therefore, both sets of data were affected by the residual stresses at the edge of the plate. A wide plate that would be more typical of a connection element is not likely to be significantly affected by the across-width residual stress pattern. In that case, the tension and compression residual stresses would need to balance for equilibrium across the thickness as shown in Figure 7c. The maximum experimental compression residual stress is estimated at 9 ksi.

The research by Alpsten (1968) and Alpsten and Tall (1969) used 2- and 3.5-in.-thick plates. For thinner plates, cooling occurs with a lower temperature gradient throughout the plate; therefore, the residual stresses in thinner plates are smaller. The simplified, linear approximation in Figure 7d will be used in the derivation of weak-axis flexural buckling strength of connection elements. The magnitude of both the tension and compression residual stresses are $0.25\sigma_y$, which is a conservative estimate based on the experimental results.

Residual stresses must be considered when assessing the inelastic buckling behavior of columns and beams. The column curve in AISC *Specification* Section E3 was developed using experimental results of rolled and welded I-shape members and box columns with various residual stress patterns. For doubly symmetric I-section members, the elastic-to-inelastic transition moment for lateral-torsional buckling in AISC *Specification* Section F2 is 70% of the yield moment. This implies a pattern with a compression residual stress of $0.3F_y$ at the flange tips, as shown in Figure 5a, which is a common pattern for elements with rolled edges. However, the different residual stress patterns created by the various fabrication processes brings uncertainty to the stability design of connection elements. Further complicating the stability design of connection elements, the buckling direction must be considered to determine whether the across-width residual stress pattern or the through-thickness pattern is applicable.

Kim and Chen (1996) and ASCE (1997) found that the AISC column curve can be closely estimated for I-shape members using a linear residual stress pattern across the flanges with a maximum compressive residual stress of $\sigma_{rc} = 0.30\sigma_y$ at the flange tips (Figure 5b). Because the residual stress pattern across the width of an I-shape flange

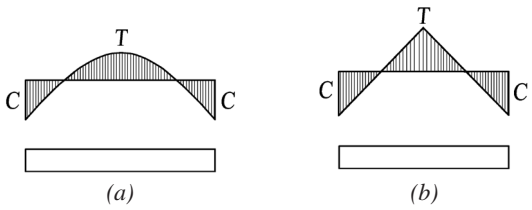

Fig. 5. Across-width residual stress pattern for bars and UM plates: (a) experimental; (b) simplified.

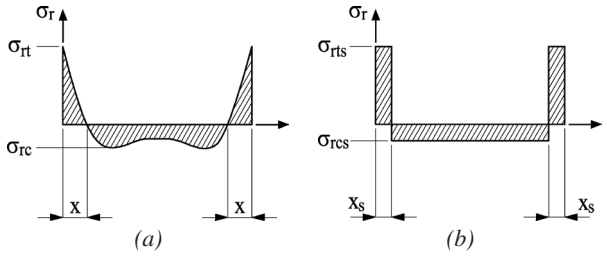

Fig. 6. Across-width residual stress pattern for plates with thermally cut edges: (a) experimental; (b) simplified.

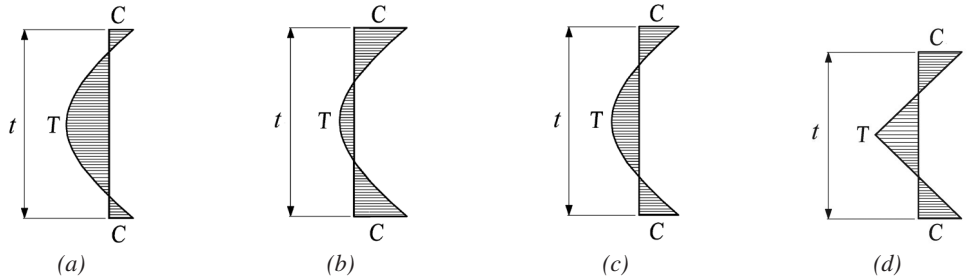

Fig. 7. Through-thickness residual stress patterns: (a) bars and UM plates; (b) flame-cut plates; (c) bars, UM plates, and flame-cut plates with large aspect ratios; (d) simplified.

is identical to that of a bar with rolled edges (Figure 5a), the strong-axis buckling behavior of a bar with rolled edges is similar to the weak-axis buckling behavior of an I-section. Therefore, for rectangular connection elements buckling about the strong axis, the effect of residual stresses is expected to be similar to that of I-shape columns. Thermally cut plates with tensile residual stress at the edges have improved buckling behavior. The stabilizing effect caused by tension residual stresses at the edges was demonstrated in the research of Bambach and Rasmussen (2002) and Rogers and Dwight (1977).

COMPRESSION STRENGTH

The flexural buckling provisions in AISC *Specification* Section E3 are reviewed, and a theoretical, tangent modulus solution is derived to analyze the differences in buckling behavior for connection elements and main members. The AISC column curve and the tangent modulus curve are compared to the available experimental results to determine their applicability to the design of connection elements.

AISC *Specification* Section J4.4

Provisions for strength of connecting elements in compression are in *Specification* Section J4.4. The available strength of connecting elements in compression for the limit states of yielding and buckling are determined as follows:

(a) When $KL/r \le 25$

$$P_n = F_y A_g \tag{1}$$

(b) When $KL/r > 25$, the provisions of Chapter E apply.

AISC *Specification* Section E3

Provisions for the flexural buckling strength of members in compression are in *Specification* Section E3. The nominal compressive strength is

$$P_n = F_{cr} A_g \tag{2}$$

The critical stress is determined as follows:

(a) When $\frac{KL}{r} \le 4.71\sqrt{\frac{E}{F_y}}$

$$F_{cr} = \left[0.658^{\left(\frac{F_y}{F_e}\right)}\right] F_y \tag{3}$$

(b) When $\frac{KL}{r} > 4.71\sqrt{\frac{E}{F_y}}$

$$F_{cr} = 0.877 F_e \tag{4}$$

where

$$F_e = \frac{\pi^2 E}{\left(\frac{KL}{r}\right)^2} \tag{5}$$

A_g = gross cross-sectional area, in.^{2}

E = modulus of elasticity, ksi

F_e = elastic buckling stress, ksi

F_y = specified minimum yield stress, ksi

K = effective length factor for flexural buckling

L = laterally unbraced length, in.

r = radius of gyration, in.

Theoretical Solutions

Using a tangent modulus approach, Galambos (1968) derived the weak-axis and strong-axis flexural buckling solutions for a rectangular column with the linear across-width residual stress pattern shown in Figure 5b. The maximum tension and compression residual stress was $0.5\sigma_y$, and the stiffness of all yielded material outside of the elastic core was neglected.

For most connection elements, the weak axis is critical for buckling, where the behavior is based on the through-thickness residual stress pattern. The tangent modulus approach from Galambos (1968) will be used to derive the buckling curve for weak-axis buckling of a plate with through-thickness residual stresses, $\sigma_{rt} = 0.25\sigma_y$ and $\sigma_{rc} = 0.25\sigma_y$. The linear approximation in Figure 7d will be used. The initial yielding condition is defined by Equation 6:

$$\sigma + \sigma_{rc} = \sigma_y \tag{6}$$

Using $\sigma_{rc} = 0.25\sigma_y$, the initial yielding stress ratio is

$$\sigma/\sigma_y = 0.75 \tag{7}$$

And the initial yielding load ratio is

$$P/P_y = 0.75 \tag{8}$$

When $P/P_y > 0.75$, the edges of the plate yield, leaving an elastic core of width, b, shown as the shaded portion in Figure 8a. Figure 8b shows the sectional stresses across the plate thickness, including the applied axial compression stress, σ, and the compression residual stress, σ_{rc}. The material behavior is defined by an elastic-perfectly plastic curve; therefore, the maximum stress on the cross-section is the material yield strength, σ_y. The elastic core is defined by a, where $b = 2\alpha t$ as shown in Figure 8b. From equilibrium of the cross section using the stress blocks in Figure 8b, the normalized load is

$$\frac{P}{P_y} = \frac{\sigma}{\sigma_y} + \frac{\sigma_{rc} - \sigma_{rt}}{2\sigma_y} - \left(\frac{\sigma + \sigma_{rc}}{\sigma_y} - 1\right)\left(\frac{1}{2} - \alpha\right) \tag{9}$$

Substitute $\sigma_{rt} = 0.25\sigma_y$ and $\sigma_{rc} = 0.25\sigma_y$ into Equation 9 to get Equation 10:

$$\frac{P}{P_y} = \frac{\sigma}{\sigma_y} - \left(\frac{\sigma}{\sigma_y} - \frac{3}{4}\right)\left(\frac{1}{2} - \alpha\right) \tag{10}$$

Using similar triangles for the stresses in Figure 8b,

$$\frac{\sigma + \sigma_{rc} - \sigma_y}{2} = \left(\sigma_{rt} + \sigma_{rc}\right)\left(\frac{1}{2} - \alpha\right) \tag{11}$$

Substitute $\sigma_{rt} = 0.25\sigma_y$ and $\sigma_{rc} = 0.25\sigma_y$ into Equation 11 to get Equation 12:

$$\frac{\sigma}{\sigma_y} = 1.25 - \alpha \tag{12}$$

Substitute Equation 12 into Equation 10 to get Equation 13:

$$\alpha = \sqrt{1 - \frac{P}{P_y}} \tag{13}$$

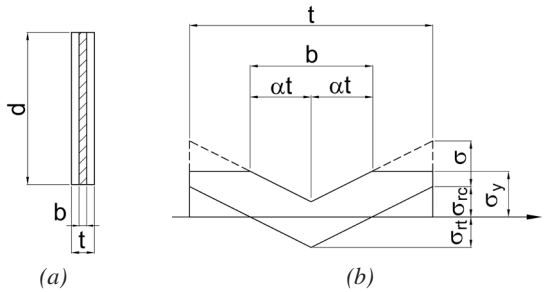

Fig. 8. Inelastic rectangular column with through-thickness residual stress pattern: (a) elastic core; (b) stresses.

The tangent modulus ratio of the cross-section is defined by τ:

$$\begin{aligned}\tau &= \frac{A_c}{A_g} \\ &= \frac{2\alpha td}{td} \\ &= 2\alpha \\ &= 2\sqrt{1 - \frac{P}{P_y}}\end{aligned} \tag{14}$$

The weak-axis moment of inertia of the plate is

$$I_y = \frac{dt^3}{12} \tag{15}$$

The weak-axis moment of inertia of the elastic core is

$$\begin{aligned}I_{yc} &= \frac{d(2\alpha t)^3}{12} \\ &= I_y\tau^3\end{aligned} \tag{16}$$

The slenderness parameter is

$$\lambda_y = \sqrt{\frac{I_{yc}/I_y}{P/P_y}} \tag{17}$$

Substituting Equation 16 into Equation 17:

$$\lambda_y = \sqrt{\frac{\tau^3}{P/P_y}} \tag{18}$$

Substituting Equation 14 into Equation 18, the slenderness parameter is given by Equation 19:

$$\lambda_y = \sqrt{\frac{8\left(1 - P/P_y\right)^{3/2}}{P/P_y}} \tag{19}$$

where

A_c = area of the elastic core, in.^{2}

P = axial load, kips

P_y = axial yield load, kips

$= A_g\sigma_y$

d = plate depth, in.

t = plate thickness, in.

σ = axial stress, ksi

σ_{rt} = tension residual stress, ksi

σ_{rc} = compression residual stress, ksi

σ_y = yield stress, ksi

The normalized load, P/P_y, versus the slenderness parameter, λ_y, for the tangent modulus solution with through-thickness residual stress is plotted in Figure 9. Because geometric imperfections are not accounted for, the tangent modulus solution follows the elastic critical load curve until $P/P_y > 0.75$. The column curve from AISC *Specification* Section E3 is also plotted. Except for very low slenderness values, the tangent modulus curve is above the AISC curve.

The tangent modulus solution for the weak-axis buckling of bars and UM plates with rolled edges can be solved using the across-width residual stress pattern of Figure 6b, with $\sigma_{rt} = 0.30\sigma_y$ and $\sigma_{rc} = 0.30\sigma_y$. The initial yielding condition is defined by Equation 6 with $\sigma_{rc} = 0.30\sigma_y$. The initial yielding load ratio is

$$P/P_y = 0.70 \tag{20}$$

When $P/P_y > 0.70$, the edges of the plate yield, leaving an elastic core of depth, h, shown as the shaded portion in Figure 10a. The elastic core is defined by the parameter, α, where $h = 2\alpha d$. Using the stresses in Figure 10b, the normalized load is

$$\frac{P}{P_y} = \frac{\sigma}{\sigma_y} + \frac{\sigma_{rc} - \sigma_{rt}}{2\sigma_y} - \left(\frac{\sigma + \sigma_{rc}}{\sigma_y} - 1\right)\left(\frac{1}{2} - \alpha\right) \tag{21}$$

Substitute $\sigma_{rt} = 0.30\sigma_y$ and $\sigma_{rc} = 0.30\sigma_y$ into Equation 21 to get Equation 22:

$$\frac{P}{P_y} = \frac{\sigma}{\sigma_y} - \left(\frac{\sigma}{\sigma_y} - 0.70\right)\left(\frac{1}{2} - \sigma\right) \tag{22}$$

Using similar triangles for the stresses in Figure 10b,

$$\frac{\sigma + \sigma_{rc} - \sigma_y}{2} = (\sigma_{rt} + \sigma_{rc})\left(\frac{1}{2} - \alpha\right) \tag{23}$$

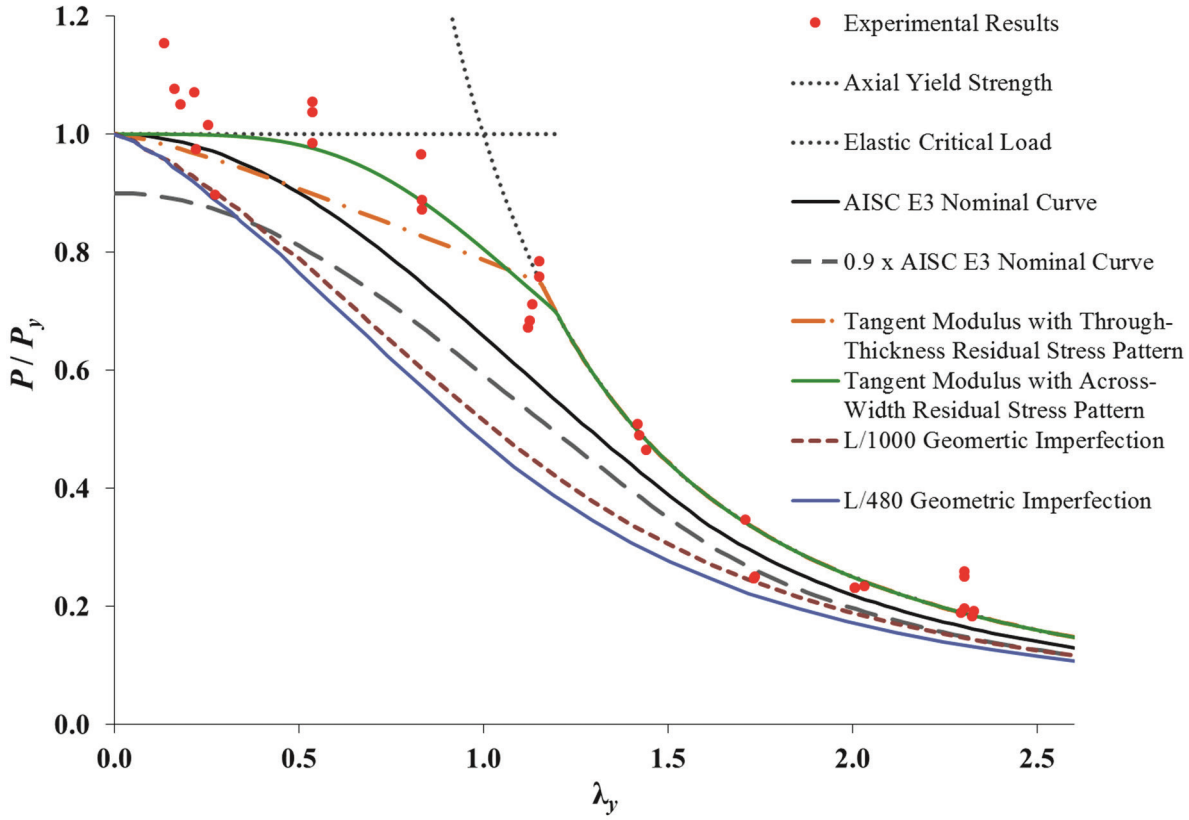

Fig. 9. Column curves for AISC Specification and theoretical solutions.

Substitute $\sigma_{rt} = 0.30\sigma_y$ and $\sigma_{rc} = 0.30\sigma_y$ into Equation 23 to get Equation 24:

$$\frac{\sigma}{\sigma_y} = 1.3 - 1.2\alpha \tag{24}$$

Substitute Equation 24 is into Equation 22 to get Equation 25:

$$\alpha = 0.913\sqrt{1 - \frac{P}{P_y}} \tag{25}$$

The tangent modulus of the cross-section is defined by τ:

$$\begin{aligned} \tau &= \frac{A_c}{A_g} \\ &= \frac{2\alpha td}{td} \\ &= 2\alpha \\ &= 1.83\sqrt{1 - \frac{P}{P_y}} \end{aligned} \tag{26}$$

The weak-axis moment of inertia of the plate is

$$I_y = \frac{dt^3}{12} \tag{27}$$

The weak-axis moment of inertia of the elastic core is

$$\begin{aligned} I_{ye} &= \frac{(2\alpha d)t^3}{12} \\ &= I_y\tau \end{aligned} \tag{28}$$

The slenderness parameter is

$$\lambda_y = \sqrt{\frac{I_{ye}/I_y}{P/P_y}} \tag{29}$$

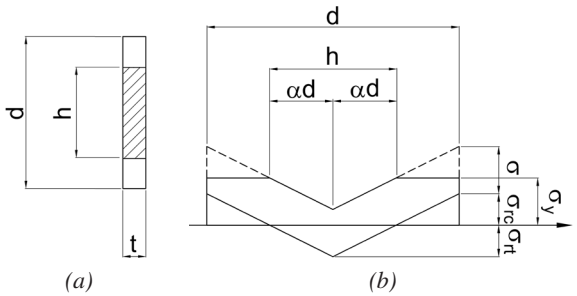

Fig. 10. Inelastic rectangular column with across-width residual stress pattern: (a) elastic core; (b) stresses.

Substituting Equation 28 into Equation 29 results in Equation 30:

$$\lambda_y = \sqrt{\frac{\tau}{P/P_y}} \tag{30}$$

Substituting Equation 26 into Equation 30, the slenderness parameter is given by Equation 31:

$$\lambda_y = 1.35\sqrt{\frac{\left(1 - P/P_y\right)^{1/2}}{P/P_y}} \tag{31}$$

The normalized load, P/P_y, versus the slenderness parameter, λ_y, for the tangent modulus solution with an across-width residual stress pattern is plotted in Figure 9. Because geometric imperfections are not accounted for, the tangent modulus solution follows the elastic critical load curve until $P/P_y > 0.70$. The tangent modulus curve is above the AISC curve for the full slenderness range.

The tangent modulus curves do not account for the initial out-of-flatness of the plate. Because the initial deformations have a negative influence on the behavior, they must be considered in the design method. A lower-bound curve for buckling of rectangular members with an initial out-of-straightness can be determined using a beam-column approach. The moment-thrust-curvature relationships by Galambos (1968) described further in the "Combined Loads" section of this paper were solved for the cases of initial mid-height out-of-straightness values of $\delta_0 = L/1{,}000$ and $\delta_0 = L/480$. The first-order moment, at the mid-height of the column is

$$M_1 = P\delta_0 \tag{32}$$

The second-order moment is

$$M_2 = \frac{M_1}{1 - \frac{P}{P_e}} \tag{33}$$

where

M_1 = first-order moment, kip-in.

M_2 = second-order moment, kip-in.

P_e = elastic critical load, kips

δ_0 = initial mid-height out-of-straightness, in.

The normalized load, P/P_y, versus the slenderness parameter, λ_y, for the moment-thrust-curvature solution by Galambos (1968) is plotted in Figure 9. The slenderness parameter is

$$\lambda_y = \frac{KL}{\pi r}\sqrt{\frac{\sigma_y}{E}} \quad (34)$$

For both out-of-straightness values, the curves are plotted in Figure 9. Both curves are similar in shape to the AISC curve; however, the theoretical solutions are well below the AISC curve for the full slenderness range. Because the derivation neglects the stiffness of all material outside the elastic core, the theoretical solution is expected to be conservative.

Experimental Comparisons

Also plotted in Figure 9 are 39 experimental results from the research projects of Seely and Putnam (1919), Haaijer (1953) and Robinson (1983), who tested small-scale solid rectangular mild steel specimens in axial compression. All of the specimens failed by flexural buckling, and the end conditions were accounted for in the calculation of the slenderness parameter, λ_y, according to Equation 34. The results are plotted as the normalized experimental load, P_t/P_y, versus the slenderness parameter. Compared to the nominal strength from AISC *Specification* Section E3, the average experimental-to-nominal load is 1.15 and the standard deviation is 0.226.

Design Recommendations

By comparing the AISC column curve to the experimental results and theoretical solutions, it can be concluded that rectangular members with proportions similar to connection elements can be designed using the flexural buckling provisions in AISC *Specification* Section E3. The resistance factor, $\phi = 0.90$, specified in Section E1 has traditionally been used to design connection elements and is adequate for isolated compression members. However, for connection elements such as the corner gusset plate shown in Figure 1, the definition of the effective width, buckling length, and effective length factor must be considered when determining the resistance factor. For example, the effective length factors proposed for gusset plate design by Dowswell (2006) were calibrated for use with $\phi = 0.90$, but Dowswell (2014) recommended using $\phi = 0.75$ to design gusset plates with a new design method with variable effective width trajectory angles.

FLEXURAL STRENGTH

The lateral-torsional buckling provisions in AISC *Specification* Section F11 are reviewed, and a theoretical, tangent modulus solution is developed to analyze the differences between connection elements and main members. Both methods are compared to the available experimental results to determine their applicability to the design of connection elements.

AISC *Specification* Section J4.5

Provisions for the strength of connecting elements in flexure are in *Specification* Section J4.5, which contains a general statement requiring the following limit states to be checked: flexural yielding, local buckling, lateral-torsional buckling, and flexural rupture. Flexural yielding and lateral-torsional buckling of rectangular connection elements can be checked using *Specification* Section F11.

For typical member design, the cross-section is made up of two or more elements; therefore, local buckling and lateral-torsional buckling are two distinct limit states. However, rectangular connection elements in flexure have a buckled shape that closely resembles lateral-torsional buckling, with lateral deformation and twisting of the cross-section. Because rectangular beams are single-element cross-sections, the local buckling limit state is not applicable.

AISC *Specification* Section F11

Provisions for the flexural strength and stability of rectangular members bent about their major axis are in *Specification* Section F11. The nominal flexural strength is

For yielding, $\frac{L_b d}{t^2} \le \frac{0.08E}{F_y}$

$$M_n = M_p = F_y Z_x \le 1.6M_y \quad (35)$$

For inelastic lateral-torsional buckling, $\frac{0.08E}{F_y} < \frac{L_b d}{t^2} \le \frac{1.9E}{F_y}$

$$M_n = C_b\left[1.52 - 0.274\left(\frac{L_b d}{t^2}\right)\frac{F_y}{E}\right]M_y \le M_p \quad (36)$$

For elastic lateral-torsional buckling, $\frac{L_b d}{t^2} > \frac{1.9E}{F_y}$

$$M_n = F_{cr} S_x \le M_p \quad (37)$$

The critical stress is

$$F_{cr} = \frac{1.9EC_b}{\frac{L_b d}{t^2}} \quad (38)$$

where

C_b = lateral-torsional buckling modification factor

E = modulus of elasticity, ksi

F_y = specified minimum yield strength, ksi

L_b = distance between brace points, in.

M_n = nominal moment, kip-in.

M_y = yield moment, kip-in.

M_p = plastic moment, kip-in.

S_x = strong-axis elastic section modulus, in.^{3}

Z_x = strong-axis plastic modulus, in.^{3}

d = beam depth, in.

t = beam width, in.

Equation 38 is the theoretical solution for the elastic critical buckling stress multiplied by C_b and simplified by substituting the properties for a rectangular cross section. It can be derived from the critical moment for a rectangular beam with equal end moments (Timoshenko and Gere, 1961):

$$M_e = \frac{\pi}{L_b}\sqrt{EI_yGJ} \tag{39}$$

where

G = shear modulus of elasticity, ksi

I_y = weak-axis moment of inertia, in.^{4}

J = torsional constant, in.^{4}

M_e = elastic critical moment, kip-in.

The critical stress is

$$F_{cr} = \frac{M_e}{S_x} \tag{40}$$

The strong-axis section modulus is

$$S_x = \frac{td^2}{6} \tag{41}$$

The weak-axis moment of inertia is

$$I_y = \frac{dt^3}{12} \tag{42}$$

The torsional constant is

$$J = \frac{dt^3}{3} \tag{43}$$

The shear modulus of elasticity is

$$G = 0.385E \tag{44}$$

Substitute Equations 42, 43 and 44 into Equation 39 and then substitute Equations 39 and 41 into Equation 40 to get

$$F_{cr} = \frac{1.95Et^2}{L_bd} \tag{45}$$

Round the constant 1.95 down to 1.9 and multiply by C_b to account for nonuniform moment to get Equation 38.

Theoretical Solutions

For cantilever beams, the inelasticity is concentrated at the fixed end of the beam, which is the location of least deformation during lateral-torsional buckling. Therefore, material inelasticity has less of a detrimental effect on cantilever beams than simply supported beams. Chakrabarti (2000) solved the differential equations for stability of a rectangular cantilever beam with a concentrated load at the free end. He determined that the beam can be considered elastic when the slenderness parameter, λ, exceeds 1.31, where λ is calculated with Equation 46. This is less conservative than AISC *Specification* Section F11, where elastic buckling is assumed for λ greater than 1.9.

$$\lambda = \frac{L_bdF_y}{Et^2} \tag{46}$$

Galambos (1968) and Galambos and Surovek (2008) derived the tangent modulus solution for inelastic lateral-torsional buckling of a rectangular beam, using only the resistance of the elastic core as shown in Figure 11. The inelastic parts of the cross section were assumed to have no torsional stiffness or weak-axis flexural stiffness. However, Neal (1950) showed, both theoretically and experimentally, that the torsional rigidity remains at the elastic value after a beam has yielded in the presence of a strong-axis moment. It was also shown that the extent of yielding has no influence on the torsional rigidity. An independent theoretical derivation by Wittrick (1952) verified Neal's conclusions. A numerical analysis by Hartmann (1971), based on the tangent modulus concept, was in agreement with the results of Neal (1950).

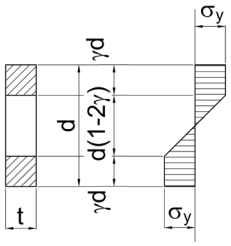

Fig. 11. Elastic core of an inelastic rectangular beam.

A new tangent modulus solution is derived here, which assumes the torsional rigidity remains at the elastic value after flexural yielding. As in the Galambos and Surovek (2008) and Neal (1950) solutions, geometric imperfections and residual stresses are neglected. The plastic moment of a rectangular cross section is

$$M_p = \frac{F_y t d^2}{4} \tag{47}$$

The weak-axis moment of inertia of the elastic core is

$$I_{yc} = \frac{t^3 d(1-2\gamma)}{12} \tag{48}$$

Substitute the sectional and material properties of Equations 43, 44 and 48 into Equation 39 to get the critical load

$$M_{cr} = \frac{0.325 E t^3 d}{L_b}\sqrt{1-2\gamma} \tag{49}$$

Divide by M_p from Equation 47 and substitute λ from Equation 46:

$$\frac{M_{cr}}{M_p} = \frac{1.30}{\lambda}\sqrt{1-2\gamma} \tag{50}$$

The depth of the yielded portion of the cross section is calculated based on the strength of the stress blocks:

$$\gamma = \frac{1}{2}\left(1-\sqrt{3-3\frac{M_{cr}}{M_p}}\right) \tag{51}$$

Substitute Equation 51 into Equation 50 to get the critical moment ratio:

$$\frac{M_{cr}}{M_p} = \frac{1.71}{\lambda}\left(1-\frac{M_{cr}}{M_p}\right)^{1/4} \tag{52}$$

Buckling is defined by the elastic critical load when $\lambda = 1.95$. This is where $M_{cr}/M_p = 2/3$, which is the S_x/Z_x ratio. The normalized moment, M_{cr}/M_p, versus the slenderness parameter, λ, for the Galambos (1968) solution and the simplified Neal solution (Equation 52) is plotted in Figure 12. The simplified Neal curve is above the Galambos curve over the entire inelastic range, showing the effect of assuming the elastic

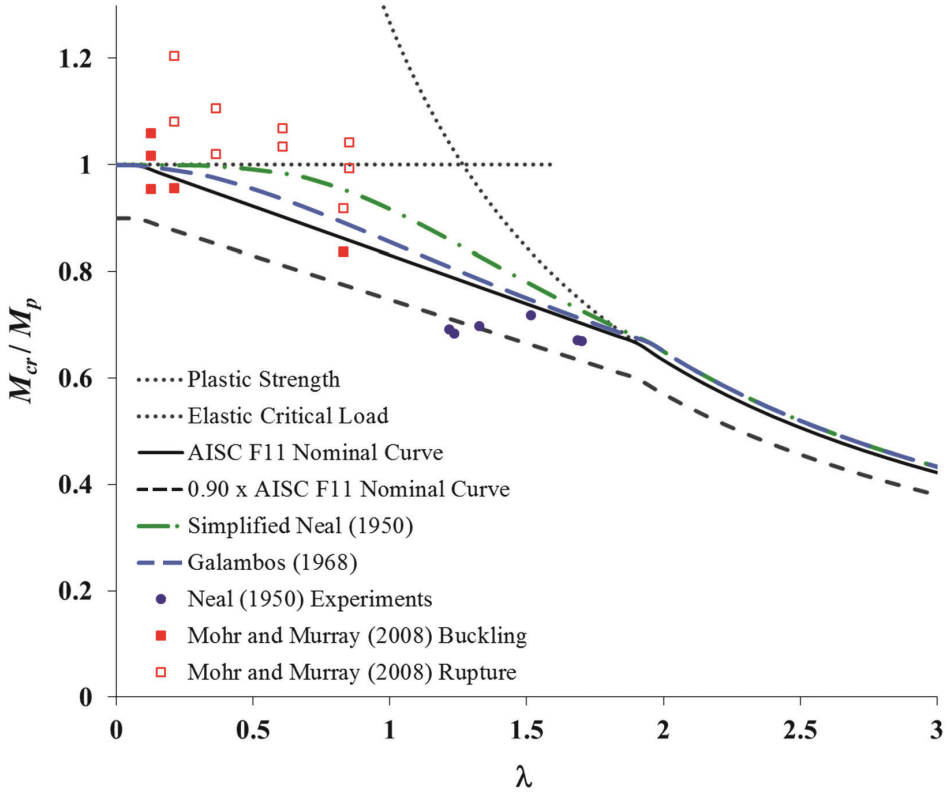

Fig. 12. Lateral-torsional buckling curves for AISC Specification and theoretical solutions.

torsional rigidity is unaffected by flexural yielding. The AISC curve consistently falls below the theoretical curves.

Experimental Comparisons

The normalized experimental moments for specimens tested by Neal (1950) and Mohr and Murray (2008) are plotted against the slenderness parameter in Figure 12. The tests by Neal were small-scale, simply supported beams with a width-to-depth ratio of 8. The results are indicated by the solid circles. The Mohr and Murray (2008) specimens were full-scale, beam web splice plates subjected to uniform moment. All six specimens by Neal (1950) and three of the five specimens by Mohr and Murray (2008) that failed by excessive deformation were below the AISC *Specification* Section F11 nominal curve. This is believed to be primarily due to the effect of geometric imperfections. For these 11 specimens, the average experimental-to-nominal load is 0.958 and the standard deviation is 0.0571.

Design Recommendations

By comparing the AISC flexural strength curve to the experimental results and theoretical solutions, it has been concluded that rectangular connection elements can be designed using the lateral-torsional buckling provisions in AISC *Specification* Section F11. The resistance factor, ϕ = 0.90, specified in Section F1, should be analyzed using further test results. Based on the limited experimental results available, with two of the specimens buckling below the available moment resistance, it appears that a lower value may be needed in some cases with uniform moment. However, this may not be justified for connection elements with a moment gradient along the length. In this case, the slightly conservative nature of Equation F1-1 in the AISC *Specification* will partially offset the need for a lower resistance factor. Also, ϕ = 0.90 may be adequate for specific connection elements where the C_b factor is calibrated using experimental or finite element results to provide the required safety index.

COMBINED LOADS

The combined loading provisions in AISC *Specification* Sections H1 and H2 are reviewed and compared to approximate theoretical solutions for rectangular members derived by Vlasov (1961), Galambos (1968) and Tomas et al. (2013), as well as to an empirical curve-fit equation proposed by Pisarenko and Mullagulov (1998). Based on these comparisons, design provisions for the buckling strength of connection elements under combined loading are recommended.

AISC *Specification* Section H1

Provisions for the load interaction of doubly symmetric members under combined flexure and compression are in *Specification* Section H1.1.

When $P_r/P_c \geq 0.2$

$$\frac{P_r}{P_c}+\frac{8}{9}\left(\frac{M_{rx}}{M_{cx}}+\frac{M_{ry}}{M_{cy}}\right)\leq 1.0 \tag{53}$$

When $P_r/P_c < 0.2$

$$\frac{P_r}{2P_c}+\frac{M_{rx}}{M_{cx}}+\frac{M_{ry}}{M_{cy}}\leq 1.0 \tag{54}$$

where

M_{cx} = available flexural strength about the strong axis, kip-in.

M_{cy} = available flexural strength about the weak axis, kip-in.

M_{rx} = required flexural strength about the strong axis, kip-in.

M_{ry} = required flexural strength about the weak axis, kip-in.

P_c = available axial strength, kips

P_r = required axial strength, kips

Specification Section H1.2 is for members under combined flexure and tension. The equations in Section H1 are used with an increase in the lateral-torsional buckling modification factor according to Equation 55.

$$C_b' = C_b\sqrt{1+\frac{\alpha P_r}{P_{ey}}} \tag{55}$$

where

$$P_{ey} = \frac{\pi^2 EI_y}{L_b^2} \tag{56}$$

α = 1.0 (LRFD); α = 1.6 (ASD)

AISC *Specification* Section H2

AISC *Specification* Section H2 provides a linear stress interaction equation that can be used for all shapes. The equation is presented in terms of stress ratios; however, for doubly symmetric members, it can be expressed using load ratios as in Equation 57:

$$\frac{P_r}{P_c}+\frac{M_{rx}}{M_{cx}}+\frac{M_{ry}}{M_{cy}}\le 1.0 \quad (57)$$

AISC *Specification* Appendix 8

The required moments used in the interaction equations in Sections H1 and H2 are second-order moments, which can be calculated using amplified first-order moments with equations similar to those in AISC *Specification* Appendix 8:

$$M_r = BM_1 \quad (58)$$

$$B=\frac{1}{1-\alpha P_r/P_e} \quad (59)$$

The elastic critical load about the bending axis is

$$P_e=\frac{\pi^2 EI}{(KL)^2} \quad (60)$$

where

B = moment amplification multiplier

M_1 = first-order moment, kip-in.

M_r = required flexural strength, kip-in.

I = moment of inertia about the bending axis, in.^{4}

Plastic Interaction

At low slenderness ratios ($\lambda_y \approx 0$), stability is not a concern, and a plastic interaction curve is applicable. For axial loading plus biaxial flexure, the equation recommended by Dowswell (2015) is

$$\left(\frac{P_r}{P_y}\right)^2+\left[\left(\frac{M_{rx}}{M_{px}}\right)^{1.7}+\left(\frac{M_{rz}}{M_{pz}}\right)^{1.7}\right]^{0.59}=1.0 \quad (61)$$

For single-axis flexure, Equation 61 reduces to

$$\left(\frac{P_r}{P_y}\right)^2+\frac{M_r}{M_p}=1.0 \quad (62)$$

Effect of Single-Axis Flexure on Axial Compression Strength

Galambos (1968) derived an approximate solution for single-axis flexure–compression interaction using inelastic moment-thrust-curvature relationships of a rectangular member. The solution accounted for instability due to flexural buckling, but not lateral-torsional buckling. The axial-moment interaction curve is defined as follows.

When $\frac{P_r}{P_y}+\left(\frac{P_r}{P_e}\right)^{1/3}>1$

$$\frac{M_r}{M_p}=2\left(1-\frac{P_r}{P_y}\right)\left[1-\left(\frac{P_r}{P_e}\right)^{1/3}\right] \quad (63)$$

When $\frac{P_r}{P_y}+\left(\frac{P_r}{P_e}\right)^{1/3}\le 1$

$$\frac{M_r}{M_p}=1-\left(\frac{P_r}{P_y}\right)^2-\left(\frac{P_r}{P_e}\right)^{2/3} \quad (64)$$

where

P_y = axial yield load, kips

$= A_g\sigma_y$

At very low slenderness ratios, $P_r/P_e \approx 0$, Equation 64 reduces to Equation 62. In Figure 13, three interaction curves are plotted for elements with a slenderness ratio of zero ($\lambda_y = 0$). These curves are defined by AISC *Specification* Section H1, AISC *Specification* Section H2, and Galambos (1968). Both of the AISC curves are well below the Galambos curve for the full loading range; however, *Specification* Section J4.4 allows the axial yield strength to be used for connecting elements in compression when $KL/r \le 25$. The Galambos curve is also plotted for $\lambda_y = 1/3$, which was selected based on $KL/r = 25$ for $F_y = 50$ ksi (at $F_y = 36$ ksi, $KL/r = 29$). It can be readily observed that the AISC *Specification* Section H1 curve for $\lambda_y = 0$ matches well with the Galambos curve for $\lambda_y = 1/3$.

The change in shape of the interaction curve with increasing λ_y is apparent in Figure 14, which shows the interaction curves for three slenderness values: $\lambda_y = 0.5$, 1.5 and 2.5. The Galambos curves are above the AISC H1 curves for most loading ranges and slenderness values; however, at high slenderness values and high moment ratios, they drop below the AISC H1 curves.

Interaction of Lateral-Torsional Buckling and Flexural Buckling

Vlasov (1961) solved the approximate differential equations for a narrow rectangular member under the action of an eccentric axial compression force applied at each end of a simply supported member. The member was restrained against torsional rotation at the ends but was free to warp. The assumed weak-axis buckled shape was a half sine wave.

The elastic critical buckling load is

$$P_{el} = \frac{P_{ey} + P_{ez}}{2H}\left[1 - \sqrt{1 - \frac{4P_{ey}P_{ez}H}{\left(P_{ey} + P_{ez}\right)^2}}\right] \quad (65)$$

The weak-axis buckling load is

$$P_{ey} = \frac{\pi^2 EI_y}{(KL)_y^2} = \frac{\pi^2 EA_g}{\left(\frac{KL}{r}\right)_y^2} \quad (66)$$

The torsional buckling load is

$$P_{ez} = \frac{GJ}{r_o^2} \quad (67)$$

where

$$H = 1 - \left(\frac{e_y}{r_x}\right)^2 \quad (68)$$

$$r_o^2 = \frac{I_x + I_y}{A_g} = \frac{t^2 + d^2}{12} \quad (69)$$

where

e_y = eccentricity in the y-direction, inducing strong-axis flexure, in.

r_x = strong-axis radius of gyration, in.

Pisarenko and Mullagulov (1998) developed an elliptical interaction equation (Equation 70) using experimental results of small-scale rectangular members under combined flexure and axial compression:

$$\left(\frac{M_r}{M_e}\right)^2 + \left(\frac{P_r}{P_{ey}}\right)^2 = 1 \quad (70)$$

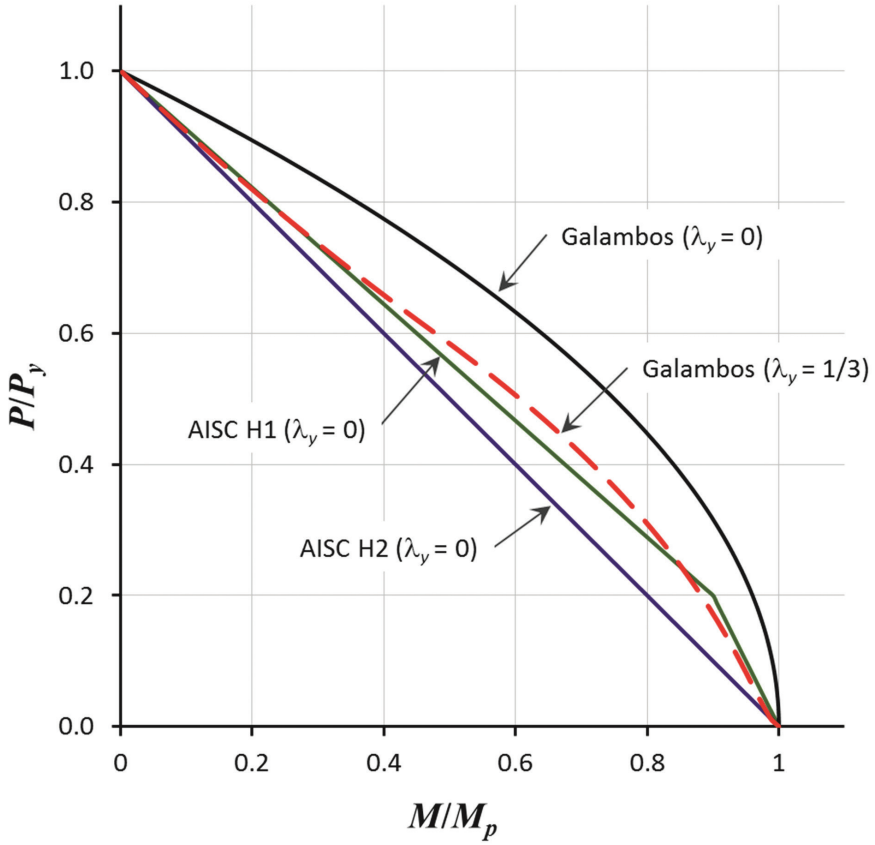

Fig. 13. Interaction curves for single-axis flexure and axial compression at low slenderness.

The elliptical and the AISC interaction equations are compared to Vlasov's (1961) solution in Figure 15. For members sized with typical beam proportions, with $L_b/d \geq 4$, elliptical interaction according to Equation 70 is conservative over most of the axial load range, with a slight nonconservatism at very high axial load ratios. The AISC interaction equations are conservative over the entire loading range. For lower length-to-depth ratios typical of connection elements, where $L_b/d \leq 2$, Equation 70 is nonconservative over much of the axial load range. Therefore, for connection elements, the AISC interaction equations are more appropriate at high axial load ratios. A more accurate solution is given by Equation 71, which is a second-order polynomial curve fit to the Vlasov (1961) solution for $L_b/d = 1$. The curve fit equation provides a good fit to the Vlasov curve, with $R^2 = 0.991$; however, the linear approximation of the Vlasov (1961) solution given by Equation 72 may be more appropriate for design purposes:

$$\frac{P}{P_{ey}} = 1 - 0.95\frac{M}{M_e} + 0.46\left(\frac{M}{M_e}\right)^2 \tag{71}$$

$$\frac{P}{P_{ey}} + 0.65\frac{M}{M_e} = 1.0 \tag{72}$$

Effect of Axial Tension on Lateral-Torsional Buckling

Tomas et al. (2013) showed that the critical buckling moment increases with the axial tension according to Equation 73:

$$M_e' = M_e\sqrt{\left(1+\frac{P_r}{P_{ey}}\right)\left(1+\frac{P_r}{P_{ez}}\right)} \tag{73}$$

By comparing Equation 73 to Equation 55, it can be observed that the AISC *Specification* equation neglects the effect of the second term under the radical in Equation 73. Numerical comparisons between the two equations showed that for rectangular members with an L/d ratio of 2 or greater, the maximum increase in critical moment due to the additional term is only 7%.

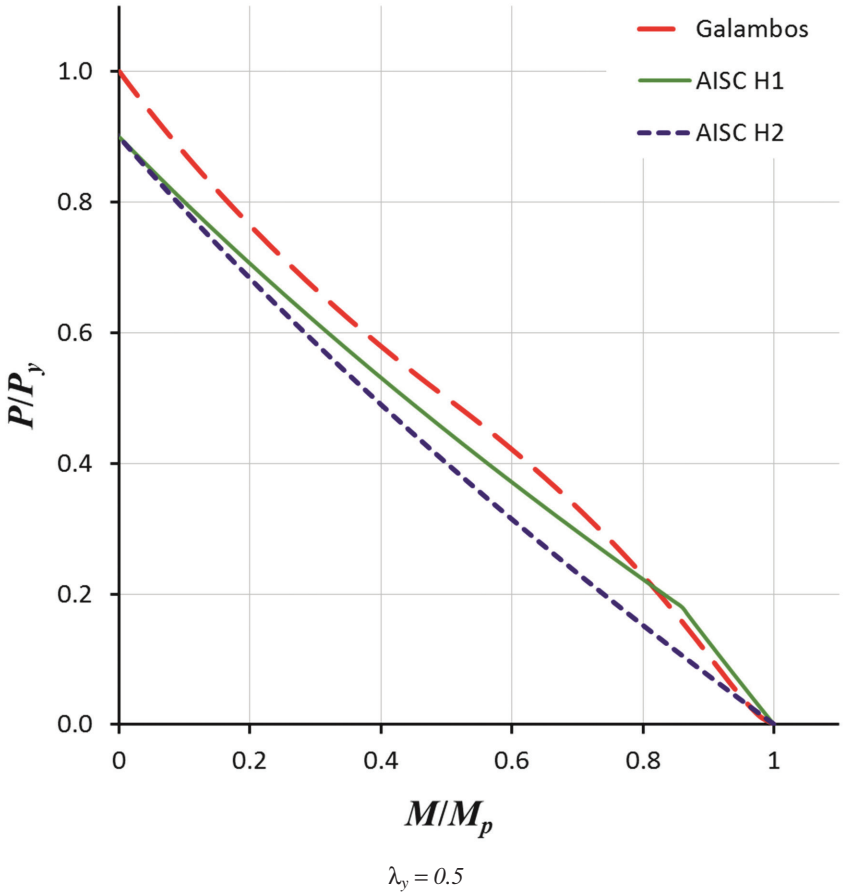

Fig. 14a. Interaction curves for single-axis flexure and axial compression at high slenderness.

Design Recommendations

By comparing the AISC load interaction curves to the theoretical solutions, it was concluded that rectangular connection elements can be designed using the following slenderness zones:

- When $\lambda_y \le 0.12$ ($KL/r \le 9.1$ for $F_y = 50$ ksi) and $M_n = M_p$, the effects of stability can be neglected and plastic interaction according to Equation 62 is applicable. This gives a maximum nonconservative error of 5%.
- When $0.12 < \lambda_y \le 0.33$ ($KL/r \le 25$ for $F_y = 50$ ksi) and $M_n = M_p$, the effects of stability can be neglected and the equations in AISC *Specification* Section H1.1 are applicable.
- When $0.33 < \lambda_y$ ($KL/r > 25$ for 50 ksi) or $M_n < M_p$, the effects of stability must be included in the design and the interaction equation in AISC *Specification* Section H2 is applicable.

For cases with combined axial tension and lateral-torsional buckling, the increased buckling resistance can be calculated with Equation 55, which is from AISC *Specification* Section H1.2. Because connection elements are often subjected to high shear demands at the same location as the maximum axial and flexural demands, an additional plastic interaction calculation may be required to determine the strength of the connection element.

CONCLUSIONS

Various factors affecting the stability of connection elements were discussed, with an emphasis on the differences between main members and connection elements. The main differences affecting the buckling strength of connection elements are smaller length-to-depth ratios, unpredictable stress distributions, ambiguous boundary conditions, different residual stress patterns, and large out-of-flatness tolerances.

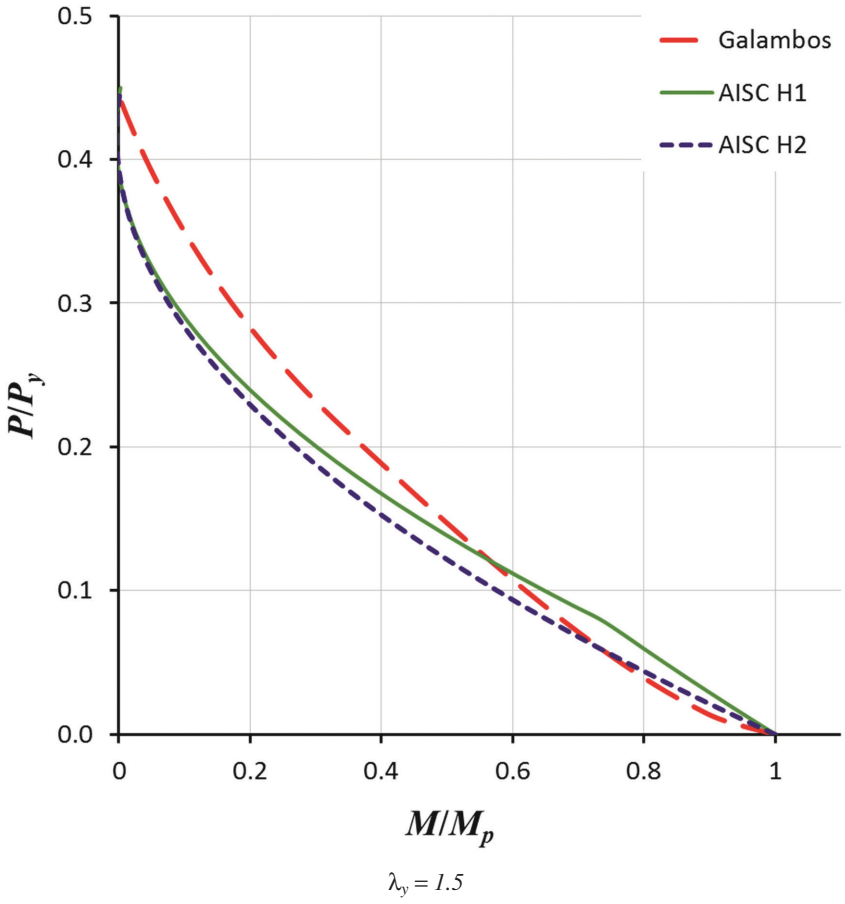

Fig. 14b. Interaction curves for single-axis flexure and axial compression at high slenderness.

A new column curve was derived, based on the tangent modulus approach, for flexural buckling of a plate with a through-thickness residual stress pattern typical of a connection element. The available data on stability of connection elements was compared to the flexural buckling, lateral-torsional buckling, and combined loading provisions in the AISC *Specification*. Based on these comparisons, practical design guidelines were recommended for the flexural buckling and lateral-torsional buckling of connection elements. It was found that rectangular connection elements can be designed using the flexural buckling provisions in AISC *Specification* Section E3 and the lateral-torsional buckling provisions in AISC *Specification* Section F11.

For combined axial-flexural loading of connection elements, it was shown that the shape of the interaction curve is dependent on the slenderness parameter, λ_y. Three slenderness zones were recommended. At low slenderness ($\lambda_y \leq 0.12$), the strength can be calculated using a plastic interaction curve. The strength of connection elements with high slenderness ($0.33 < \lambda_y$) is best predicted with AISC *Specification* Section H2. At intermediate slenderness ($0.12 < \lambda_y \leq 0.33$), the effects of stability can be neglected and the interaction equations in AISC *Specification* Section H1.1 are applicable. For cases with combined axial tension and lateral-torsional buckling, the increased buckling resistance can be calculated with the equation in AISC *Specification* Section H1.2.

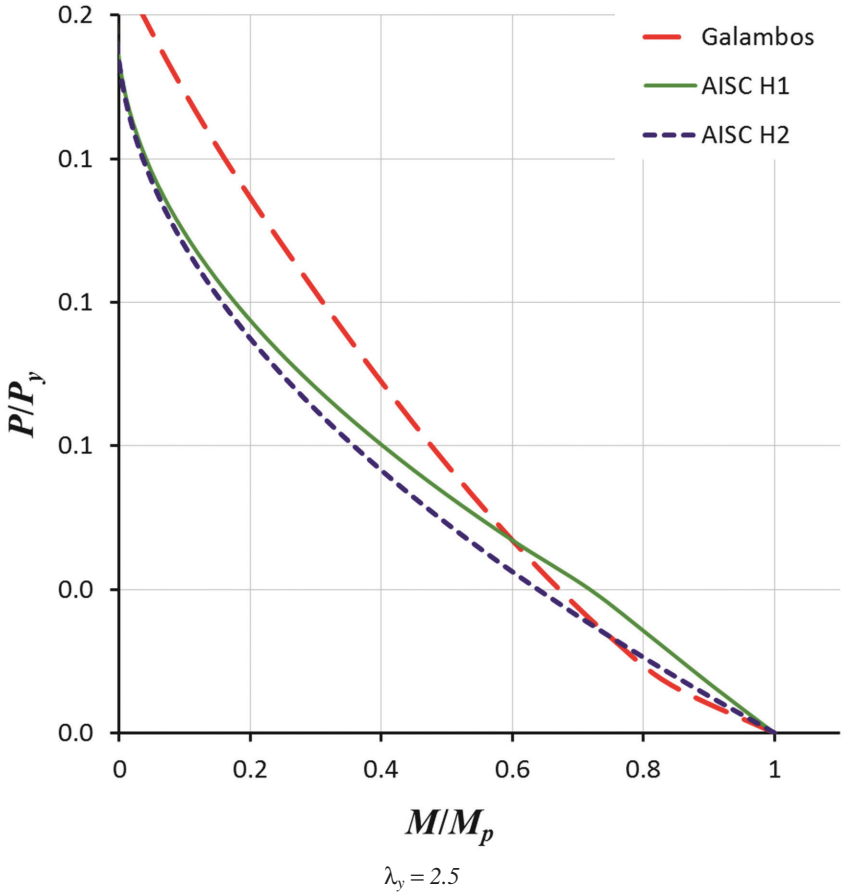

Fig. 14c. Interaction curves for single-axis flexure and axial compression at high slenderness.

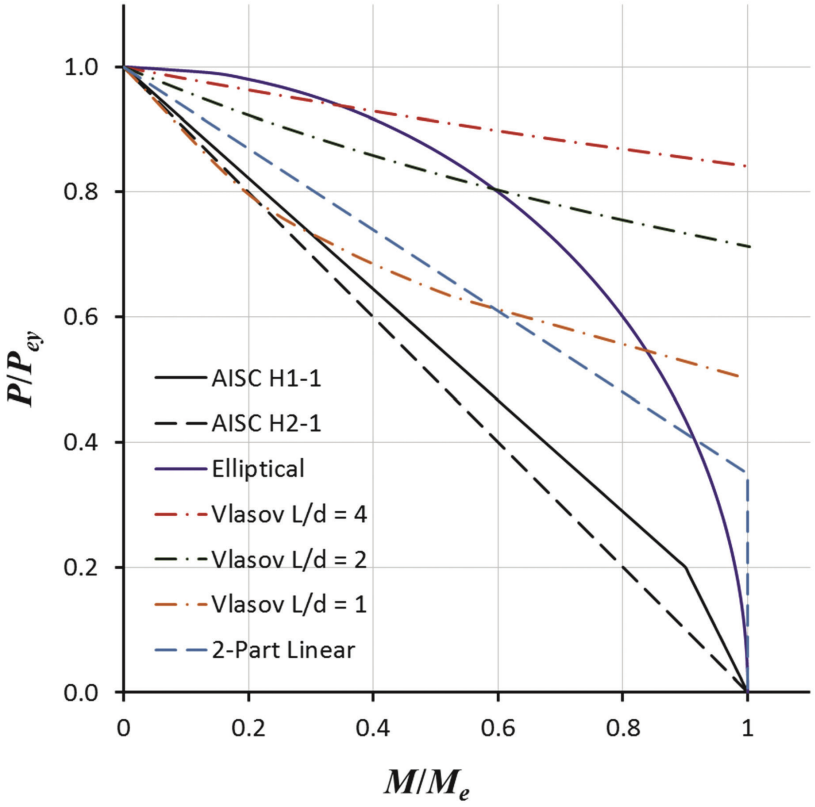

Fig. 15. Interaction curves for lateral-torsional buckling and flexural buckling.

DESIGN EXAMPLES

Coped Beam Example 1

In this example, the cope buckling strength will be calculated for a double-coped W18×50 beam subjected to shear and axial compression. The cope is 4½ in. long × 1½ in. deep at both flanges as shown in Figure 16. The beam material is ASTM A992, and the beam is braced laterally by a floor slab at the face of the top-flange cope.

ASTM A992: $F_y = 50$ ksi

W18×50: $t_w = 0.355$ in. $d = 18.0$ in.

Cope length: $c = c_t = c_b = 4½$ in.

Cope depth: $d_c = d_{ct} = d_{cb} = 1½$ in.

Distance from the face of the cope to the end reaction: $e = 4½$ in.

Reduced depth of web, $h_o = 18.0$ in. − (2)(1½ in.) = 15.0 in.

The vertical and horizontal reactions are:

LRFD	ASD
$R_u = 90$ kips	$R_a = 60$ kips
$F_{tu} = 120$ kips	$F_{ta} = 80$ kips

The moment at the face of the cope is $M = Re$:

LRFD	ASD
$M_u = R_u e$	$M_u = R_u e$
$= (90 \text{ kip})(4½ \text{ in.})$	$= (60 \text{ kip})(4½ \text{ in.})$
= 405 kip-in.	= 270 kip-in.

Flexural Strength

From Dowswell and Whyte (2014), for beams with equal cope lengths at the top and bottom flange, C_b is

$$C_b = \left[3 + \ln\left(\frac{L_b}{d}\right)\right]\left(1 - \frac{d_{ct}}{d}\right) \le 1.84$$

$$= \left[3 + \ln\left(\frac{4½ \text{ in.}}{18.0 \text{ in.}}\right)\right]\left(1 - \frac{1½ \text{ in}}{18.0 \text{ in}}\right) \le 1.84$$

$$= 1.48$$

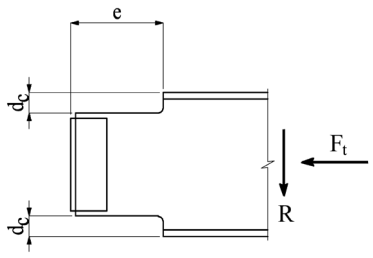

Fig. 16. Coped beam for Examples 1 and 2.

AISC *Specification* Section F11 is used with $C_b = 1.48$ and $L_b = c_t = 4½$ in. (Dowswell and Whyte, 2014):

$$M_y = (50 \text{ ksi})\left[\frac{(0.355 \text{ in.})(15.0 \text{ in.})^2}{6}\right]$$
$$= 666 \text{ kip-in.}$$

$$M_p = (50 \text{ ksi})\left[\frac{(0.355 \text{ in.})(15.0 \text{ in.})^2}{4}\right]$$
$$= 998 \text{ kip-in.}$$

$$\frac{L_b d}{t^2} = \frac{(4½ \text{ in.})(18.0 \text{ in.})}{(0.355 \text{ in.})^2}$$
$$= 643$$

$$\frac{0.08E}{F_y} = \frac{(0.08)(29{,}000 \text{ ksi})}{(50 \text{ ksi})}$$
$$= 46.4$$

$$\frac{1.9E}{F_y} = \frac{(1.9)(29{,}000 \text{ ksi})}{(50 \text{ ksi})}$$
$$= 1{,}100$$

$$46.4 < 643 < 1{,}100$$

Therefore, the nominal flexural strength is

$$M_n = C_b\left[1.52 - 0.274\left(\frac{L_b d}{t^2}\right)\frac{F_y}{E}\right]M_y \le M_p$$
$$= (1.48)\left[1.52 - (0.274)(643)\left(\frac{50 \text{ ksi}}{29{,}000 \text{ ksi}}\right)\right](666 \text{ kip-in.}) \le 998 \text{ kip-in.}$$
$$= 998 \text{ kip-in.}$$

LRFD	ASD
$\phi M_n = (0.9)(998 \text{ kip-in.})$ $= 898 \text{ kip-in.}$	$\frac{M_n}{\Omega} = \frac{998 \text{ kip-in.}}{1.67}$ $= 598 \text{ kip-in.}$

Axial Strength

$$A_g = h_o t_w$$
$$= (15.0 \text{ in.})(0.355 \text{ in.})$$
$$= 5.33 \text{ in.}^2$$

$$\frac{KL}{r} = \frac{(0.5)(4\frac{1}{2}\text{ in.})}{(0.355\text{ in.})/\sqrt{12}}$$
$$= 22.0$$

$22.0 < 25$

Therefore, according to *Specification* Section J4.4,

$$P_n = F_y A_g$$
$$= (50\text{ ksi})(5.33\text{ in.}^2)$$
$$= 267\text{ kips}$$

LRFD	ASD
$\phi P_n = (0.9)(267\text{ kips})$ $= 240\text{ kips}$	$\frac{P_n}{\Omega} = \frac{267\text{ kips}}{1.67}$ $= 160\text{ kips}$

Stability Interaction

When $0.12 < \lambda_y \le 0.33$ ($KL/r \le 25$ for $F_y = 50$ ksi) and $M_n = M_p$, the effects of stability can be neglected and the interaction equation in AISC *Specification* Section H1.1 is applicable.

LRFD	ASD
$\frac{P_r}{P_c} = \frac{P_u}{\phi P_n}$ $= \frac{120\text{ kips}}{240\text{ kips}}$ $= 0.500$	$\frac{P_r}{P_c} = \frac{P_a}{P_n/\Omega}$ $= \frac{80\text{ kips}}{160\text{ kips}}$ $= 0.500$

Because $0.500 \ge 0.2$, according to *Specification* Section H1.1,

$$\frac{P_r}{P_c} + \frac{8}{9}\left(\frac{M_{rx}}{M_{cx}}\right) \le 1.0$$

LRFD	ASD
$0.500 + \frac{8}{9}\left(\frac{405\text{ kip-in.}}{898\text{ kip-in.}}\right) = 0.901 < 1.0$	$0.500 + \frac{8}{9}\left(\frac{270\text{ kip-in.}}{598\text{ kip-in.}}\right) = 0.901 < 1.0$

Therefore, the cope is adequate for the limit state of local stability.

Coped Beam Example 2

In this example, the cope buckling strength will be calculated for a double-coped W18×50 beam subjected to shear and axial compression. The cope is 18 in. long × 1½ in. deep at both flanges as shown in Figure 16. The beam material is ASTM A992, and the beam is braced laterally by a floor slab at the face of the top-flange cope.

ASTM A992: $F_y = 50$ ksi

W18×50: $t_w = 0.355$ in. $d = 18.0$ in.

Cope length: $c = c_t = c_b = 18$ in.

Cope depth: $d_c = d_{ct} = d_{cb} = 1½$ in.

Distance from the face of the cope to the end reaction: $e = 18$ in.

Reduced depth of web, $h_o = 18.0$ in. $- (2)(1½$ in.$) = 15.0$ in.

The vertical and horizontal reactions are shown here:

LRFD	ASD
$R_u = 15$ kips	$R_a = 10$ kips
$F_{tu} = 45$ kips	$F_{ta} = 30$ kips

The moment at the face of the cope is $M = Re$:

LRFD	ASD
$M_u = R_u e$	$M_u = R_u e$
$= (15 \text{ kip})(18 \text{ in.})$	$= (10 \text{ kip})(18 \text{ in.})$
$= 270$ kip-in.	$= 180$ kip-in.

Flexural Strength

From Dowswell and Whyte (2014), for beams with equal cope lengths at the top and bottom flange, C_b is

$$C_b = \left[3 + \ln\left(\frac{L_b}{d}\right)\right]\left(1 - \frac{d_{ct}}{d}\right) \le 1.84$$

$$= \left[3 + \ln\left(\frac{18 \text{ in.}}{18.0 \text{ in.}}\right)\right]\left(1 - \frac{1½ \text{ in}}{18.0 \text{ in}}\right) \le 1.84$$

$$= 1.84$$

AISC *Specification* Section F11 is used with $C_b = 1.84$ and $L_b = c_t = 18$ in. (Dowswell and Whyte, 2014):

$$S_x = \frac{(0.355 \text{ in.})(15.0 \text{ in.})^2}{6}$$

$$= 13.3 \text{ in.}^3$$

$$M_p = (50 \text{ ksi})\left[\frac{(0.355 \text{ in.})(15.0 \text{ in.})^2}{4}\right]$$

$$= 998 \text{ kip-in.}$$

$$\frac{L_b d}{t^2} = \frac{(18 \text{ in.})(18.0 \text{ in.})}{(0.355 \text{ in.})^2}$$

$$= 2{,}570$$

$$\frac{1.9E}{F_y} = \frac{(1.9)(29{,}000 \text{ ksi})}{(50 \text{ ksi})}$$
$$= 1{,}100$$

$1{,}100 < 2{,}570$

Therefore, the critical stress is

$$F_{cr} = \frac{1.9EC_b}{\frac{L_b d}{t^2}}$$
$$= \frac{(1.9)(29{,}000 \text{ ksi})(1.84)}{2{,}570}$$
$$= 39.4 \text{ ksi}$$

The nominal flexural strength is

$$M_n = F_{cr} S_x \le M_p$$
$$= (39.4 \text{ ksi})(13.3 \text{ in.}^3)$$
$$= 524 \text{ kip-in.}$$

LRFD	ASD
$\phi M_n = (0.9)(524 \text{ kip-in.})$ $= 472 \text{ kip-in.}$	$\frac{M_n}{\Omega} = \frac{542 \text{ kip-in.}}{1.67}$ $= 314 \text{ kip-in.}$

Axial Strength

$$A_g = h_o t_w$$
$$= (15.0 \text{ in.})(0.355 \text{ in.})$$
$$= 5.33 \text{ in.}^2$$

$$\frac{KL}{r} = \frac{(0.5)(18 \text{ in.})}{(0.355 \text{ in.})/\sqrt{12}}$$
$$= 87.8$$

$87.8 > 25$

Therefore, the axial strength will be calculated according to the provisions of *Specification* Chapter E. The elastic buckling stress is

$$F_e = \frac{\pi^2 E}{\left(\frac{KL}{r}\right)^2}$$
$$= \frac{\pi^2 (29{,}000 \text{ ksi})}{(87.8)^2}$$
$$= 37.1 \text{ ksi}$$

The slenderness parameter is

$$4.71\sqrt{\frac{E}{F_y}} = 4.71\sqrt{\frac{29{,}000 \text{ ksi}}{50 \text{ ksi}}}$$
$$= 113$$
$$47.8 < 113$$

Therefore, the critical buckling stress is

$$F_{cr} = \left[0.658^{\left(\frac{50 \text{ ksi}}{37.1 \text{ ksi}}\right)}\right](50 \text{ ksi})$$
$$= 28.4 \text{ ksi}$$

The nominal compressive strength is

$$P_n = F_{cr} A_g$$
$$= (28.4 \text{ ksi})(5.33 \text{ in.}^2)$$
$$= 151 \text{ kips}$$

LRFD	ASD
$\phi P_n = (0.9)(151 \text{ kips})$ $= 136 \text{ kips}$	$\frac{P_n}{\Omega} = \frac{151 \text{ kips}}{1.67}$ $= 90.4 \text{ kips}$

Stability Interaction

When $0.33 < \lambda_y$ ($KL/r > 25$ for 50 ksi) or $M_n < M_p$, the effects of stability must be included in the design, and the interaction equation in AISC *Specification* Section H2 is applicable. Due to the high flexural stiffness in the strong-axis direction, the strong-axis second-order moment is neglected.

LRFD	ASD
$\frac{P_r}{P_c} + \frac{M_{rx}}{M_{cx}} \le 1.0$	$\frac{P_r}{P_c} + \frac{M_{rx}}{M_{cx}} \le 1.0$
$\frac{45 \text{ kip}}{136 \text{ kip}} + \frac{270 \text{ kip-in.}}{472 \text{ kip-in.}} = 0.903 < 1.0$	$\frac{30 \text{ kip}}{90.4 \text{ kip}} + \frac{180 \text{ kip-in.}}{314 \text{ kip-in.}} = 0.905 < 1.0$

Therefore, the cope is adequate for the limit state of local stability.

Coped Beam Example 3

In this example, the cope buckling strength will be calculated for a double-coped W18×50 beam subjected to shear and axial tension. The cope is 18 in. long × 1½ in. deep at both flanges as shown in Figure 17. The beam material is ASTM A992, and the beam is braced laterally by a floor slab at the face of the top-flange cope.

ASTM A992: $F_y = 50$ ksi

W18×50: $t_w = 0.355$ in. $d = 18.0$ in.

Cope length: $c = c_t = c_b = 18$ in.

Cope depth: $d_c = d_{ct} = d_{cb} = 1½$ in.

Distance from the face of the cope to the end reaction: $e = 18$ in.

Reduced depth of web, $h_o = 18.0$ in. − (2)(1½ in.) = 15.0 in.

The vertical and horizontal reactions are:

LRFD	ASD
$R_u = 21$ kips	$R_a = 14$ kips
$F_{tu} = 120$ kips	$F_{ta} = 80$ kips

The moment at the face of the cope is $M = Re$:

LRFD	ASD
$M_u = R_u e$	$M_u = R_u e$
$= (21 \text{ kip})(18 \text{ in.})$	$= (14 \text{ kip})(18 \text{ in.})$
$= 378$ kip-in.	$= 252$ kip-in.

Flexural Strength

From Dowswell and Whyte (2014), for beams with equal cope lengths at the top and bottom flange, C_b is

$$C_b = \left[3 + \ln\left(\frac{L_b}{d}\right)\right]\left(1 - \frac{d_{ct}}{d}\right) \le 1.84$$
$$= \left[3 + \ln\left(\frac{18 \text{ in.}}{18.0 \text{ in.}}\right)\right]\left(1 - \frac{1½ \text{ in.}}{18.0 \text{ in.}}\right) \le 1.84$$
$$= 1.84$$

Specification Section H1.2 will be used to calculate the effect of the tension load on the lateral-torsional buckling strength.

$$I_y = \frac{h_o t_w^3}{12}$$
$$= \frac{(15.0 \text{ in.})(0.355 \text{ in.})^3}{12}$$
$$= 0.0559 \text{ in.}^4$$

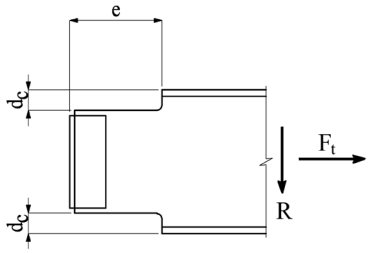

Fig. 17. Coped beam for Example 3.

$$P_{ey} = \frac{\pi^2 EI_y}{L_b^2}$$
$$= \frac{\pi^2 \left(29{,}000 \text{ ksi}\right)\left(0.0559 \text{ in.}^4\right)}{\left(18 \text{ in.}\right)^2}$$
$$= 49.4 \text{ kips}$$

According to Equation 60:

LRFD	ASD
$C_b' = 1.84\sqrt{1 + \frac{(1.0)(120 \text{ kips})}{49.4 \text{ kips}}}$	$C_b' = 1.84\sqrt{1 + \frac{(1.6)(80 \text{ kips})}{49.4 \text{ kips}}}$
$= 3.41$	$= 3.49$

AISC *Specification* Section F11 is used with $C_b = 3.41$ (LRFD), $C_b = 3.49$ (ASD), and $L_b = c_t = 18$ in. (Dowswell and Whyte, 2014):

$$S_x = \frac{\left(0.355 \text{ in.}\right)\left(15.0 \text{ in.}\right)^2}{6}$$
$$= 13.3 \text{ in.}^3$$
$$M_p = \left(50 \text{ ksi}\right)\left[\frac{\left(0.355 \text{ in.}\right)\left(15.0 \text{ in.}\right)^2}{4}\right]$$
$$= 998 \text{ kip-in.}$$

$$\frac{L_b d}{t^2} = \frac{\left(18 \text{ in.}\right)\left(18.0 \text{ in.}\right)}{\left(0.355 \text{ in.}\right)^2}$$
$$= 2{,}570$$

$$\frac{1.9E}{F_y} = \frac{(1.9)(29{,}000 \text{ ksi})}{\left(50 \text{ ksi}\right)}$$
$$= 1{,}100$$

$1{,}100 < 2{,}570$

Therefore, the critical stress is

LRFD	ASD
$F_{cr} = \frac{1.9EC_b}{\frac{L_b d}{t^2}}$	$F_{cr} = \frac{1.9EC_b}{\frac{L_b d}{t^2}}$
$= \frac{(1.9)(29{,}000 \text{ ksi})(3.41)}{2{,}570}$	$= \frac{(1.9)(29{,}000 \text{ ksi})(3.49)}{2{,}570}$
$= 73.1 \text{ ksi}$	$= 74.8 \text{ ksi}$

The nominal flexural strength is

LRFD	ASD
$M_n = F_{cr}S_x \le M_p$ $= (73.1 \text{ ksi})(13.3 \text{ in.}^3)$ $= 972 \text{ kip-in.}$	$M_n = F_{cr}S_x \le M_p$ $= (74.8 \text{ ksi})(13.3 \text{ in.}^3)$ $= 995 \text{ kip-in.}$

LRFD	ASD
$\phi M_n = (0.9)(972 \text{ kip-in.})$ $= 875 \text{ kip-in.}$	$\frac{M_n}{\Omega} = \frac{995 \text{ kip-in.}}{1.67}$ $= 596 \text{ kip-in.}$

Axial Strength

$$A_g = h_o t_w$$
$$= (15.0 \text{ in.})(0.355 \text{ in.})$$
$$= 5.33 \text{ in.}^2$$
$$P_n = F_y A_g$$
$$= (50 \text{ ksi})(5.33 \text{ in.}^2)$$
$$= 267 \text{ kips}$$

LRFD	ASD
$\phi P_n = (0.9)(267 \text{ kips})$ $= 240 \text{ kips}$	$\frac{P_n}{\Omega} = \frac{267 \text{ kips}}{1.67}$ $= 160 \text{ kips}$

Stability Interaction

When $0.33 < \lambda_y$ ($KL/r > 25$ for 50 ksi) or $M_n < M_p$, the effects of stability must be included in the design, and the interaction equation in AISC *Specification* Section H2 is applicable.

$$\frac{P_r}{P_c} + \frac{M_{rx}}{M_{cx}} \le 1.0$$

LRFD	ASD
$\frac{P_r}{P_c} + \frac{M_{rx}}{M_{cx}} \le 1.0$ $\frac{120 \text{ kip}}{240 \text{ kip}} + \frac{378 \text{ kip-in.}}{875 \text{ kip-in.}} = 0.932 < 1.0$	$\frac{P_r}{P_c} + \frac{M_{rx}}{M_{cx}} \le 1.0$ $\frac{80 \text{ kip}}{160 \text{ kip}} + \frac{252 \text{ kip-in.}}{596 \text{ kip-in.}} = 0.923 < 1.0$

Therefore, the cope is adequate for the limit state of local stability.

SYMBOLS

A_c area of the elastic core, in.^{2}

A_g gross cross-sectional area, in.^{2}

B moment amplification multiplier

C_b lateral-torsional buckling modification factor

C_w warping constant, in.^{6}

E modulus of elasticity, ksi

F_{cr} critical buckling stress, ksi

F_e elastic buckling stress, ksi

F_y specified minimum yield stress, ksi

G shear modulus of elasticity, ksi

H flexural constant

I moment of inertia about the bending axis

I_x strong-axis moment of inertia, in.^{4}

I_y weak-axis moment of inertia, in.^{4}

I_{yc} weak-axis moment of inertia of the elastic core, in.^{4}

J torsional constant, in.^{4}

K effective length factor for flexural buckling

K_t torsion parameter

L laterally unbraced length for lateral buckling, in.

L_b distance between brace points for lateral-torsional buckling, in.

M_1 first-order moment, kip-in.

M_2 second-order moment, kip-in.

M_A absolute value of moment at quarter point of the unbraced segment, kip-in.

M_B absolute value of moment at centerline of the unbraced segment, kip-in.

M_C absolute value of moment at three-quarter point of the unbraced segment, kip-in.

M_{cx} available flexural strength about the strong axis, kip-in.

M_{cy} available flexural strength about the weak axis, kip-in.

M_e elastic critical buckling moment, kip-in.

$M_{\max}$ absolute value of maximum moment in the unbraced segment, kip-in.

M_n nominal moment, kip-in.

M_p plastic moment, kip-in.

M_r required flexural strength, kip-in.

M_{rx} required flexural strength about the strong axis, kip-in.

M_{ry} required flexural strength about the weak axis, kip-in.

M_y nominal strong-axis yield moment, kip-in.

P axial load, kips

P_c available axial strength, kips

P_e elastic critical buckling load, kips

P_{el} elastic critical buckling load for an eccentrically loaded compression member, kips

P_{ey} elastic weak-axis critical buckling load, kips

P_{ez} elastic torsional critical buckling load, kips

P_r required axial strength, kips

P_y axial yield load, kips

R_m cross-section monosymmetry parameter

S_x strong-axis elastic section modulus, in.^{3}

Z_x strong-axis plastic modulus, in.^{3}

b width of elastic core, in.

d plate depth, in.

e_y eccentricity in the y-direction, inducing strong-axis flexure, in.

r radius of gyration, in.

r_o polar radius of gyration, in.

r_x strong-axis radius of gyration, in.

t plate thickness, in

x_s width of the rectangular tension block in the simplified residual stress pattern

α elastic core dimensional parameter

δ_0 initial mid-height out-of-straightness, in.

γ depth of the yielded portion of the cross section

λ slenderness parameter for lateral-torsional buckling

λ_y slenderness parameter for flexural buckling

σ axial stress, ksi

σ_{rc} compression residual stress, ksi

σ_{rt} tension residual stress, ksi

σ_y yield stress, ksi

τ ratio of tangent modulus to elastic modulus

REFERENCES

AISC (1997), *Hollow Structural Sections Connections Manual,* American Institute of Steel Construction, Chicago, IL.

AISC (2010a), *Specification for Structural Steel Buildings*, ANSI/AISC 360-10, American Institute of Steel Construction, Chicago, IL.

AISC (2010b), *Code of Standard Practice for Steel Buildings and Bridges*, American Institute of Steel Construction, Chicago, IL.

AISC (2011), *Steel Construction Manual*, 14th Ed., American Institute of Steel Construction, Chicago, IL.

Albermani, F., Khoo, X. and Perera, M. (2009), "Design of Eccentrically Connected Cleat Plates in Compression," *Proceedings of the Sixth International Conference on Advances in Steel Structures*, Hong Kong, China, The Hong Kong Institute of Steel Construction.

Alpsten, G.A. (1968), "Thermal Residual Stresses in Hot-Rolled Steel Members," Report No. 337.3, Fritz Engineering Laboratory, Lehigh University, Bethlehem, PA.

Alpsten, G.A. and Tall, L. (1969), "Residual Stresses in Thick Welded Plates," Report No. 337.12, Fritz Engineering Laboratory, Lehigh University, Bethlehem, PA.

ASCE (1997), *Effective Length and Notional Load Approaches for Assessing Frame Stability: Implications for American Steel Design*, American Society of Civil Engineers, Reston, VA.

ASTM (2013), *Standard Specification for General Requirements for Rolled Structural Steel Bars, Plates, Shapes, and Sheet Piling*, ASTM A6, ASTM International, West Conshohocken, PA.

Bambach, M.R. and Rasmussen, K.J.R. (2002, May), "Tests of Unstiffened Elements Under Combined Compression and Bending," Research Report No. R818, Center for Advanced Structural Engineering, The University of Sydney.

Bjorhovde, R. (1988), "Columns: From Theory to Practice," *Engineering Journal,* AISC, Vol. 25, No. 1, First Quarter, pp. 21–34.

Bjorhovde, R., Brozzetti, J., Alpsten, G.A. and Tall, L. (1972), "Residual Stresses in Thick Welded Plates," *Welding Research Supplement,* August, pp. 392-s – 405-s.

Bjorhovde, R., Engstrom, M.F., Griffis, L.G., Kloiber, L.A. and Malley, J.O. (2001), *Structural Steel Selection Considerations — A Guide for Students, Educators, Designers, and Builders*, American Society of Civil Engineers, Reston, VA.

Blehaut, H., Gognau, D., Flahaut, P. Khouchaf, L. and Hariri, S. (2002), "Characterisation of the Effects of Grinding on Residual Stresses," *Materials Science Forum*, Vol. 404–407, pp. 179–184.

Chakrabarti J. (2000), *Applied Plasticity,* Springer, New York, NY.

Cheng, J.J., Yura, J.A. and Johnson, C.P. (1984, July), "Design and Behavior of Coped Beam," Ferguson Lab Report, The University of Texas at Austin.

Clifton, G.C. (2006, July), "Design Procedure for Eccentrically Loaded Cleats in Compression," HERA Design and Construction Bulletin No. 80, Heavy Engineering Research Association, Manukau City, New Zealand.

Clifton, G.C., Mago, N. and El Sarraf, R. (2007), "Eccentric Cleats in Compression and Columns in Moment-Resisting Connections," HERA Report R4-142:2007, Heavy Engineering Research Association, Manukau City, New Zealand.

Dowswell, B. (2005), *Design of Steel Gusset Plates with Large Cutouts*, Ph.D. Dissertation, University of Alabama at Birmingham.

Dowswell, B. (2006), "Effective Length Factors for Gusset Plate Buckling," *Engineering Journal*, AISC, Vol. 43, No. 2, Second Quarter.

Dowswell, B. (2012a), "Effective Length Factors for Chevron Gusset Plates," *Engineering Journal*, AISC, Vol. 49, No 3, Third Quarter.

Dowswell, B. (2012b), "Connection Design for Industrial Structures—Problems and Solutions," *Proceedings of the Structures for Mining and Related Materials Handling Conference*, South African Institute of Steel Construction, October 15–18, Vanderbijlpark, South Africa.

Dowswell, B. (2014), "Gusset Plate Stability Using Variable Stress Trajectories," *Proceedings of the ASCE/SEI Structures Congress,* April 3–5, Boston, MA.

Dowswell, B. (2015), "Plastic Strength of Connection Elements," *Engineering Journal*, AISC, Vol. 52, No. 1, First Quarter.

Dowswell, B. and Whyte, R. (2014), "Local Stability of Double-Coped Beams," *Engineering Journal*, AISC, Vol. 51, No. 1, First Quarter.

Dwight, J.B. and Moxham, K.E. (1977), "Comprehensive Strength of Welded Plates," *Stability of Structures Under Static and Dynamic Loads*, ASCE, pp. 463–480.

Dwight, J.B. and Ractliffe, A.T. (1967), "The Strength of Thin Plates in Compression," *Thin Walled Steel Structures-Their Design and Use in Building*, Crosby Lockwood & Son, LTD., London, pp. 3–34.

Fouad, F.H., Davidson, J.S., Delatte, N., Calvert, E.A., Chen, S., Nunez, E. and Abdalla, R. (2003), "Structural Supports for Highway Signs, Luminaries, and Traffic Signals," NCHRP Report 494, Transportation Research Board, Washington, DC.

Galambos, T.V. (1968), *Structural Members and Frames*, Prentice-Hall, New York, NY.

Galambos, T.V. and Surovek, A.E. (2008), *Structural Stability of Steel*, John Wiley and Sons, New York, NY.

Harris, I.D. (1997), "Plasma Arc Cutting of Bridge Steels," Report 384, National Cooperative Highway Research Program, National Academy Press, Washington, DC.

Haaijer, G. (1953, June 15), "Welded Continuous Frames and Their Components-Progress Report S," Fritz Laboratory Report No. 205E-2, Lehigh University, Bethlehem, PA.

Hartmann, A.J. (1971), "Inelastic Flexural-Torsional Buckling," *Journal of the Engineering Mechanics Division*, ASCE, Vol. 97, No. EM4, pp. 1,103–1,119.

Harvey, J.F. (1985), *Theory and Design of Pressure Vessels*, Van Nostrand Reinhold Co., New York, NY.

Hogan, T.J. and Collins, R.T. (2010), "Design Model for Light Bracing Cleat Connections," *Steel Construction*, Australian Steel Institute, Vol. 43, No. 2, pp. 3–56.

Kim, S.E. and Chen, W.F. (1996), "Practical Advanced Analysis for Braced Steel Frame Design," *Journal of Structural Engineering*, ASCE, Vol. 122, No. 11, pp. 1,266–1,274.

McFalls, R.K. and Tall, L. (1969), "A Study of Welded Columns Manufactured from Flame-Cut Plates," *Welding Research Suplement,* April, pp. 141-s – 153-s.

Mohr, B.A. and Murray, T.M. (2008), "Bending Strength of Steel Bracket and Splice Plates," *Engineering Journal*, AISC, Vol. 45, No. 2, Second Quarter.

Neal, B.G. (1950), "The Lateral Instability of Yielded Mild Steel Beams of Rectangular Cross-Section," *Philosophical Transactions of the Royal Society of London*, Vol. 242, No. 846, pp. 197–242.

Packer, J. Sherman, D. and Lecce, M. (2010), *Hollow Structural Section Connections*, Design Guide 24, AISC, Chicago, IL.

Pisarenko, G.S. and Mullagulov, M.K. (1998), "Approximate Method for the Analysis of Stability of Beams Under the Action of a System of Longitudinal and Transverse Forces," *Strength of Materials*, Vol. 30, No. 3, pp. 291–298.

Rao, N. and Tall, L. (1961), "Residual Stresses in Welded Plates," *Welding Research Supplement,* October, pp. 468-s–480-s.

Robinson, S. (1983), *Failure of Steel Gusset Plates*, Ph.D. Dissertation, Department of Civil Engineering and Construction, The University of Ashton in Birmingham, Birmingham, AL.

Rogers, N.A. and Dwight, J.B. (1977), "Outstand Strength," *Steel Plated Structures, An International Symposium*, Granada Publishing LTD, London.

Seely, F.B. and Putnam, W.K. (1919, November 10), *The Relation Between the Elastic Strengths of Steel in Tension, Compression and Shear*, Bulletin No. 115, Engineering Experiment Station, Vol. 17, No. 11, University of Illinois, Champaign-Urbana, IL.

Spragen, W. and Claussen, G.E. (1937), "Shrinkage Stresses in Welding, A Review of Literature to January 1, 1937," *Welding Research Supplement*, November.

Tall, L. (1964), "Residual Stresses in Welded Plates," *Welding Research Supplemen*t, January, pp. 10-s–23-s.

Thornton, W.A. (1984), "Bracing Connections for Heavy Construction," *Engineering Journal*, AISC, Vol. 21, No. 3, Third Quarter, pp. 139–148.

Timoshenko, S.P. and Gere, J.M. (1961), *Theory of Elastic Stability*, 2nd Ed., McGraw-Hill, New York, NY.

Tomas, J., Nseir, J., Camotim, D. and Boissonnade, N. (2013), "Stability, Failure and Design of I-Section Steel Beams Subjected to Tension," *Proceedings of the Annual Stability Conference,* St. Louis, MO., April 16–20, Structural Stability Research Council, pp. 669–695.

Vlasov, V. Z. (1961), *Thin-Walled Elastic Beams*, 2nd Ed., National Science Foundation, Washington, DC.

Wilkinson, T., Stock, D. and Hastie, A. (2010), "Eccentric Cleat Plate Connections in Hollow Section Members in Compression," *Proceedings: Tubular Structures XIII*, The University of Hong Kong.

Wittrick, W.H. (1952), "Lateral Instability of Rectangular Beams of Strain-Hardening Material Under Uniform Bending," *Journal of the Areonautical Sciences*, Vol. 119, No. 12, pp. 835–843.

Young, B.W. and Dwight, J.B. (1971), *Residual Stresses and their Effect on the Moment Curvature Properties of Structural Steel Sections*, CIRIA Technical Note 32, London.